# Continuous cultivation of the lithoautotrophic nitrate-reducing Fe(II)-oxidizing culture KS in a chemostat bioreactor

*T. Bayer[1], E.J. Tomaszewski[1,†], C. Bryce[2], A. Kappler[1,3] and J.M. Byrne[2,*]*

[1]Geomicrobiology Group, Center for Applied Geoscience, University of Tuebingen, Schnarrenbergstraße 94-96, 72076 Tuebingen, Germany.

[†] **Current address:** U.S. Geological Survey, 3215 Marine St. Boulder, CO 80303 USA.

[2]School of Earth Sciences, University of Bristol, Queens Road BS8 1RJ, Bristol, United Kingdom.

[3]Cluster of Excellence: EXC 2124: Controlling Microbes to Fight Infection, Tuebingen, Germany.

***Correspondence:**
James M. Byrne
james.byrne@bristol.ac.uk

**Running title:** Culture KS cultivation in a chemostat

**Keywords**: Fe(II) oxidation; nitrite; cell encrustation; autotrophic; NRFeOx

## Originality-Significance Statement

We cultivated the chemolithoautotrophic nitrate-reducing Fe(II)-oxidizing culture KS continuously in a chemostat for 24 days and revealed the previously undetected processes of nitrite production and cell encrustation. We provide a new cultivation method for Fe(II)-oxidizing microorganisms and shed light into the mechanisms of nitrate-reducing Fe(II) oxidation, questioning the exclusivity of enzymatic activity of autotrophic nitrate-reducing Fe(II)-oxidizing microorganisms.

**Summary**

Laboratory-based studies on microbial Fe(II) oxidation are commonly performed over just a few weeks in small volumes with high substrate concentrations, resulting in geochemical gradients and volumetric effects caused by sampling. We used a chemostat to enable uninterrupted supply of medium, and investigated autotrophic growth of the nitrate-reducing Fe(II)-oxidizing culture KS for 24 days. We analysed Fe- and N-speciation, cell-mineral associations, and the identity of minerals. Results were compared to different batch systems (50 and 700 ml – static/shaken). The Fe(II) oxidation rate was highest in the chemostat with 7.57 mM Fe(II) $d^{-1}$, while the extent was similar (averaged 92% of all Fe(II)). Short-range ordered Fe(III) phases, presumably ferrihydrite, precipitated and later goethite was detected in the chemostat. 1 mM solid phase Fe(II) remained in the chemostat, up to 15 µM of reactive nitrite was measured, and 42% of visualized cells were partially or completely mineral-encrusted, likely caused by abiotic oxidation of Fe(II) by nitrite. Despite (partial) encrustation, cells were still viable. Our results show that even with similar oxidation rates as in batch cultures, cultivating Fe(II)-oxidizing microorganisms under continuous conditions reveals mechanistic insights on the role of reactive intermediates for Fe(II) oxidation, mineral formation and cell-mineral interactions.

**Abstract art:**

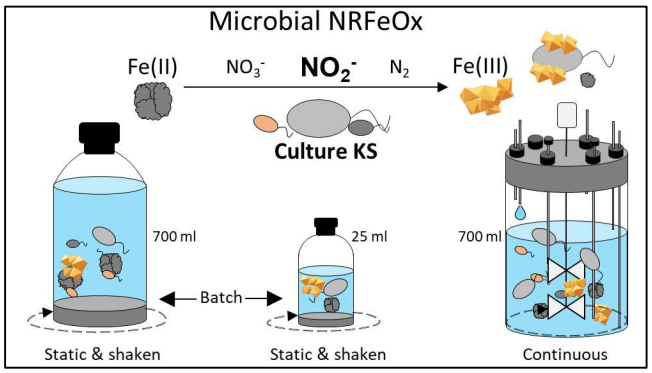

## Introduction

Iron (Fe) is one of the most abundant elements in the environment and essential to almost all known organisms, either as nutrient or as electron donor/acceptor (Boyd and Ellwood, 2010; Kendall et al., 2012). Fe is commonly present as ferrous (Fe(II)) or ferric iron (Fe(III)) (Cornell and Schwertmann, 2003; Kappler et al., 2021a) and redox cycling takes place abiotically (e.g. via light or organic matter) or by microbial metabolisms (Hedrich et al., 2011; Kappler et al., 2021b). Fe(II)-oxidizing bacteria at circumneutral pH use Fe(II) as an electron donor to reduce electron acceptors such as $O_2$, $CO_2$, or nitrate (Bryce et al., 2018). Microaerophilic Fe(II)-oxidizing bacteria compete with abiotic Fe(II) oxidation at low $O_2$-concentrations (Emerson and Moyer, 1997; Druschel et al., 2008; Maisch et al., 2019), while anaerobic phototrophic Fe(II)-oxidizers use light energy to reduce and fix $CO_2$ (Widdel et al., 1993; Ehrenreich and Widdel, 1994). Finally, nitrate-reducing Fe(II)-oxidizing (NRFeOx) bacteria couple Fe(II) oxidation to the reduction of nitrate ($NO_3^-$) in anoxic environments (Straub et al., 1996; Weber et al., 2006; Roden, 2012). Over the past three decades, NRFeOx microorganisms were intensely studied for metabolic flexibility, microbial community composition and interactions (Straub et al., 1996; He et al., 2016), and in terms of their implications for $NO_3^-$-removal in environments impacted by N-fertilizers commonly used in agriculture (Kim et al., 2015; Ward et al., 2018; Visser et al., 2021). NRFeOx microorganisms have been found in different environments, including freshwater ponds and lakes, brackish-waters, marine sediments, and aquifers (Hafenbradl et al., 1996; Straub et al., 1998; Finneran et al., 2002; Emmerich et al., 2012; Melton et al., 2012; Liu et al., 2019b; Jakus et al., 2021a). NRFeOx microorganisms stepwise reduce $NO_3^-$ to nitrogen ($N_2$) or ammonium ($NH_4^+$). This process involves multiple intermediates like $NO_2^-$, NO, and $N_2O$ (Tiedje, 1988; Straub et al., 1996; Canfield et al., 2010; Coby et al., 2011). The first enriched microbial consortium capable of chemolithoautotrophic

NRFeOx (i.e. using Fe(II) as inorganic electron donor to fix $CO_2$), was described by Straub et al. (1996) as the co-culture "culture KS". Only two additional autotrophic co-cultures have been enriched since (Huang et al., 2021b; Jakus et al., 2021b). The term "co-culture" describes a consortium of different microorganisms, meaning it is not a pure culture. Autotrophically grown culture KS is dominated by *Gallionellaceae* sp. (96%), which is considered the main Fe(II)-oxidizer, but also contains *Rhodanobacter* (1%) and *Bradyrhizobium* (1%) (Blöthe and Roden, 2009; He et al., 2016). Most other NRFeOx microorganisms can only be cultivated in the presence of an additional organic substrate (Benz et al., 1998; Kappler et al., 2005; Laufer et al., 2016; Liu et al., 2019a), as demonstrated e.g. for *Acidovorax* sp. BoFeN1 (Muehe et al., 2009). There is no conclusive evidence that these microorganisms gain energy by Fe(II) oxidation, or if they are chemodenitrifiers (Bryce et al., 2018). This lack of evidence suggests that Fe(II) oxidation, at least to some extent, could be caused by abiotic side reactions with the reactive nitrogen species (RNS) $NO_2^-$ and NO (Kampschreur et al., 2011), which can abiotically oxidize Fe(II) (Betlach and Tiedje, 1981; Klueglein and Kappler, 2013; Klueglein et al., 2014). Exclusive oxidation of Fe(II) by RNS is described as abiotic chemodenitrification (Dhakal et al., 2013). Whenever RNS are present, NRFeOx microorganisms compete with abiotic oxidation (Klueglein et al., 2014). This makes differentiating abiotic processes from NRFeOx activity a challenging task. In order to identify, quantify, and disentangle different Fe(II) oxidation mechanisms, conditions must be as steady and controllable as possible. However, common laboratory experiments studying NRFeOx are usually performed in stationary batch systems with high substrate concentrations (10s of mM) to allow cell growth and regular sampling without significant decrease of volume. High concentrations can lead to toxic effects (Swanner et al., 2015) and usually result in rapid concentration changes of nutrients and electron donors/acceptors during cultivation. Furthermore, the time scale of

closed system experiments for Fe(II)-oxidizing bacteria rarely exceed 1-2 weeks. Therefore, these experiments are inherently limited in how much volume can be removed for measurements, the long-term investigation of microbial activity, and how environmentally representative they can be. Conversely, continuous cultivation using a chemostat enables cultivation over prolonged time scales (Weusthuis et al., 1994), and provides constant supply and steady concentrations of substrates and nutrients. Enabling the addition of fresh growth-medium while removing waste products and metabolites should therefore allow establishment of a steady state. Additionally, several geochemical and physical parameters can be monitored non-invasively and controlled (pH, dissolved oxygen, and temperature). A chemostat therefore eliminates the analytical and temporal limitations of batch experiments, and can be used to further elucidate Fe(II) oxidation mechanisms to better understand mineral transformation, the fate of contaminants like $NO_3^-$ (Borch et al., 2009) and the coupling of biogeochemical cycles (Peiffer et al., 2021). In this study, we established a chemostat bioreactor as an alternative cultivation method and examined continuous autotrophic growth of NRFeOx culture KS. We compared culture KS grown autotrophically in the chemostat bioreactor in 700 ml volume for 24 days to four different batch conditions: Shaken and static in small and large volume (25 ml and 700 ml, respectively). We measured changes in concentrations of Fe and N species over time. We analysed biogenic Fe(III) minerals using µ-X-ray diffraction (µ-XRD), Moessbauer spectroscopy, and X-ray absorption spectroscopy (XAS), and visualised cell-mineral-associations with scanning electron microscopy (SEM).

## Materials and Methods

### Bacterial strain, pre-cultivation and growth conditions

Culture KS, obtained from the culture collection of the Tuebingen Geomicrobiology Group, was pre-grown twice for 7 days under autotrophic conditions with 10 mM Fe(II) and 4 mM

$NO_3^-$ on bicarbonate-buffered (22 mM) basal medium, as previously described (Tominski et al., 2018). All experiments were performed with 10 mM Fe(II) as $FeCl_2$ and 4 mM $NO_3^-$ as $NaNO_3$ for batch system. For the chemostat, fresh medium with the same substrate concentrations was continuously supplied (see below).

**Chemicals and materials**

All chemicals were at least of analytical grade. The water used was ultra-pure (Milli-Q, A10, Merck-Millipore, Billerica, USA). Anoxic solutions were prepared by either purging with $N_2$ or $N_2/CO_2$ and stored in glass containers sealed with butyl stoppers. All utensils and glassware were sterilized by autoclaving (121°C for 20 min) or by baking in an oven (180°C for 4.5 h).

**Setup of the chemostat and batch experiments**

In the chemostat, culture KS was cultivated in a volume of 700 ml inside a glass vessel (New Brunswick Scientific, USA) (Figure 1). Medium was exchanged at a rate of 15 ml·$h^{-1}$ (i.e. 2.1% exchange·$h^{-1}$, v/v) and agitated with an impeller rotating at 50 rpm. The growth medium, reaction chamber and waste-collection systems were interconnected and continuously flushed with $N_2/CO_2$ (90:10 v/v %) at 10 mbar overpressure, to maintain anoxic conditions and provide inorganic carbon (Figure 1, Figure S1). Anoxia was confirmed with a dissolved oxygen (DO) sensor (Mettler-Toledo AG, Urdorf, Switzerland) and an oxygen sensitive foil with a Fibox 3 optode oxygen measurement device (Presens, Germany). Prior to inoculating, the glass vessel was visually inspected for brownish oxidation rings at the liquid's surface, typically associated with abiotic Fe(II) oxidation. Temperature, pH, and DO were measured *in-situ* (Figures S1 and S2). For pumping in and out of the reaction vessel, external peristaltic pumps (MS-MC/CA 4, Ismatec, Germany) were used. The output was set to a slightly lower rate than the input, to maintain constant volume despite sampling. A conductivity- activated pump was triggered when the volume in the bioreactor reached 710 ml, decreasing it back to 700 ml.

Further information on setting up the chemostat can be found in the supplementary information (text SI). Batch experiments were conducted in biological triplicates in liquid volumes of either 25 ml or 700 ml. Separate triplicates of each volume were conducted for either static or shaken (50 rpm) conditions, allowing comparison of more traditional culturing experiments and shaken systems with the chemostat (Figure 1). An abiotic control (no bacteria added) was performed for all batch experiments. All biotic experiments were inoculated with 1% (v/v) of a pre-grown culture KS (as described) (Tominski et al., 2018). To prevent out-diluting the small volume of added bacteria due to the pumping in the chemostat, it was only turned on after sampling after 24 h.

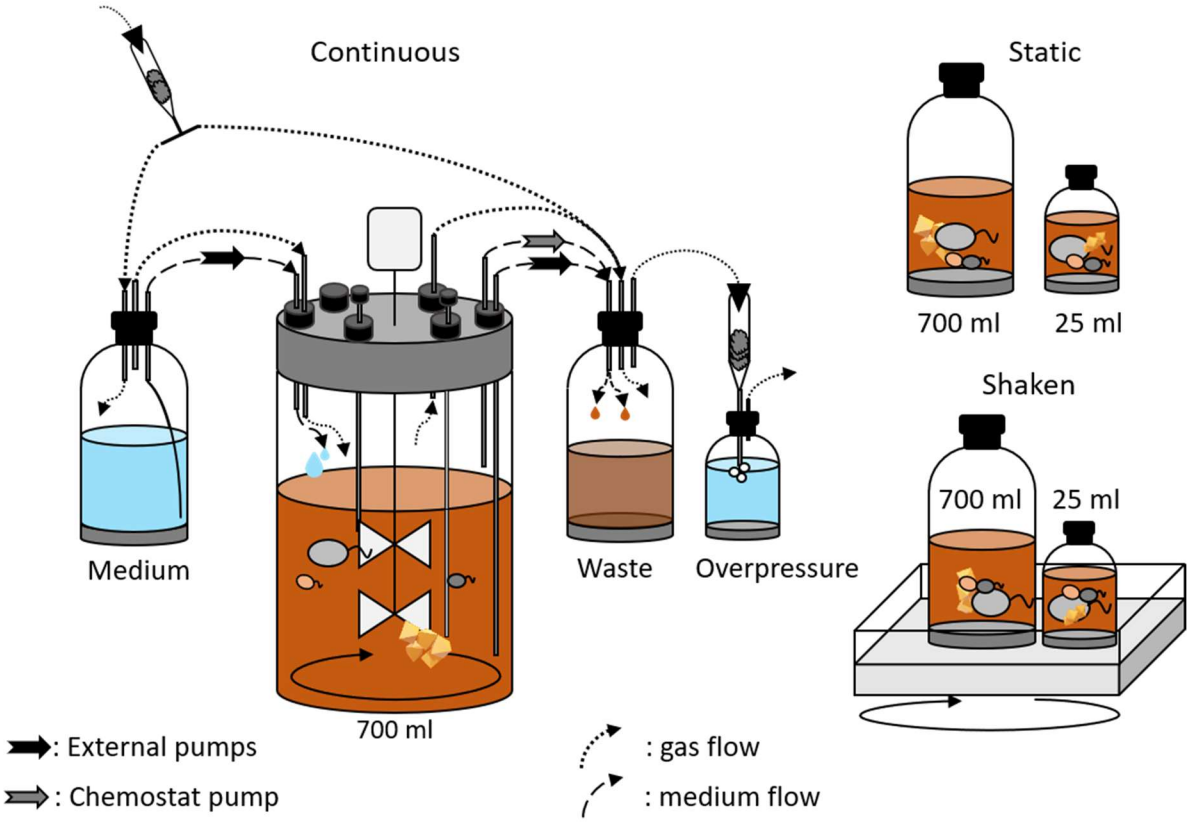


***Figure 1.*** *Schematic overview of the setup of the chemostat. Arrows indicate flow of gas or liquids. All parts were connected and inoculated under sterile conditions. The chemostat chamber and all connected bottles were flushed with $N_2/CO_2$ to keep the system anoxic and to provide inorganic carbon. Control experiments were conducted in small and big volumes (25 ml and 700 ml medium, respectively) in static or shaken (50 rpm) conditions*

**Geochemical analyses and Fe(II) oxidation rates**

Samples from the chemostat were transferred with syringe and needle into a sterile, anoxic glass vial and brought into a glovebox (100% $N_2$, MBraun Germany). Batch experiments were sampled in the glovebox. Under anoxic conditions, 1 ml was pipetted into an Eppendorf tube and centrifuged (minispin, Eppendorf) for 10 minutes at 13.4k rpm. The sample was split into the supernatant and pellet for aqueous and solid phase Fe ($Fe_{aq}$ and $Fe_s$ respectively), $NO_3^-$, and $NO_2^-$ analyses. For $Fe_{aq}$, supernatant was 10x diluted in 40 mM sulfamic acid in 1 M hydrochloric acid (1M $HCl_{SA}$) to prevent Fe(II) oxidation by RNS (Klueglein et al., 2014; Schaedler et al., 2017). For $NO_3^-$, supernatant was 20x diluted in anoxic Milli-Q. For $NO_2^-$, 750 µl were separated into a new Eppendorf tube. All samples were stored anoxically at 4°C until measurement. The pellet was dissolved for 1 h in 1 ml of anoxic 6 M $HCl_{SA}$ for $Fe_s$ measurements. Fe(II) and total Fe (Fe(T)) were determined using the spectrophotometric ferrozine assay as described by Stookey (1970) but adapted for microtiter plates (96 well assay Plate, COStar, Kennebunk, USA). Absorbance was measured at 562 nm using a plate reader (Multiskan$^{TM}$ GO Microplate Spectrophotometer, Thermo Scientific). $NO_3^-$ and $NO_2^-$ were measured using a continuous-flow analyser (Seal Analytical; Norderstedt, Germany) with a dialysis membrane for iron removal. Here, $NO_3^-$ is reduced to $NO_2^-$ with a solution of hydrazine sulphate, and then concentrations are determined photometrically with N-1-naphtyethylendiamin at a wavelength of 520 nm. The maximum Fe(II) oxidation rates in batch setups were determined from the difference between Fe(II) concentrations across consecutive timepoints. The calculated Fe(II) oxidation rate in the chemostat was adjusted to account for the continuous addition of Fe(II) from the supply bottle containing medium, which was continuously stirred to avoid enrichment of precipitated Fe(II) phases (see figure S3 and text SI for more information).

**Mineralogical and microscopic analyses**

For Moessbauer spectroscopy, 8 ml of sample was transferred to the glovebox. Minerals were collected by filtration through a 0.45 µm pore-size syringe filter (Millipore membrane). The filter was then embedded between two layers of Kapton tape foil and stored frozen (-20°C) and anoxically until analysis. Samples were inserted into a closed-cycle exchange gas cryostat (SHI-650-5; Janis Research, USA). Spectra were collected at 77 K using a constant acceleration drive system (WissEI, Blieskastel, Germany). Gamma radiation was emitted by a $^{57}$Co-source embedded in a rhodium matrix. Sample spectra were calibrated against a 7-µm-thick Fe(0) foil at room temperature. The Recoil software (University of Ottawa, Canada) was used for fitting spectra using the Voigt-based fitting model. The Lorentzian half-width-half-maximum (HWHM) value was kept constant at 0.133 mm/s. The sample spectra were analysed with respect to the isomer shift (δ) values and the quadrupole splitting ($\Delta E_Q$) and the Gaussian width (standard deviation) of the $\Delta E_Q$ was used to account for line broadening until the fit was reasonable. For µ-XRD, samples were collected and air dried in an Eppendorf tube in an oven at 27°C inside an anoxic glovebox. µ-XRD was performed on the dried material using Bruker's D8 Discover GADDS XRD2 micro-diffractometer equipped with a standard sealed tube with Co-cathode (Co Kα radiation, λ = 0.154 nm; 30 kV/30 mA). The total measurement time was 240 s at two detector positions, 15° and 40°. Phase identification was validated using Match! software version 3.6.2.121 with Crystallography Open Database (COD-Inorg REV211633 2018.19.25). For X-ray adsorption spectroscopy (XAS), an anoxically dried sample taken after 40 days (no geochemistry measured) was diluted with polyvinylpyrrolidone and pressed into 7-mm pellets using a KBr pellet press (International Crystal). The pellet was anoxically sealed in Kapton tape. X-ray absorption spectroscopy was performed at the Advanced Photon Source (APS) Materials Research Collaborative Access Team (MRCAT) beamline 10-ID-B at Argonne

National Laboratory (Segre et al., 2000). Beamline 10-ID-B employs an undulator magnet source and a Si(111) monochromator. Spectra were collected at the Fe K-edge (7.112 keV) to k=0-16 $Å^{-1}$. Data reduction, normalization and calibration were performed using the ATHENA program in the Demeter software package (Ravel and Newville, 2005). The spectrum was calibrated to a Fe reference foil spectrum collected during data collection. Linear combination fitting (LCF) of $k^3$ weighted Fe EXAFS spectra was performed from k=3-12 $Å^{-1}$ using ferrihydrite, siderite, goethite, and lepidocrocite spectra collected at the same beamline. Other standards considered during fitting include a ferrihydrite-humic acid co-precipitate, a Fe(II)-natural organic matter co-precipitate and a Fe(III)-citrate complex, all of which were collected previously at various beamlines (Shimizu et al., 2013; Daugherty et al., 2017). This type of fitting offers a semi-quantitative approach to understand the contribution of various Fe phases. SIXpack (Webb, 2005) software was used to perform LCF analysis. Samples for scanning electron microscopy were fixed in 2.5% glutaraldehyde overnight at 4°C. After washing three times with DI-water, samples were applied to a Poly-L-Lysine coated glass slide. Dehydration was performed on the glass slides by stepwise water replacement with increasing concentrations of pure ethanol (30, 50, 70, 90, and 2x 100 %), followed by washing in hexamethyldisilazane twice for 30 seconds. Samples were then mounted onto SEM aluminium stubs using double sided spectra-carbon tape (Plano, Germany) and sputter coated with a 12 nm platinum layer (Baltec SCD005 sputter-coater). Micrographs were collected using a JEOL JSM-6500F field emission SEM with a Schottky-field-emitter at a working distance of approximately 10 mm at the Centre for Light-Matter Interaction, Sensor & Analytics ($LISA^+$), University of Tuebingen.

## Results and discussion

### Iron(II) oxidation and $NO_2^-$ production during growth of culture KS

We quantified concentrations of Fe(II), Fe(T), as well as $NO_3^-$ and $NO_2^-$ during autotrophic growth of culture KS (Figure 2, Figures S4-S11). Results indicated that Fe was initially only present as Fe(II), with the majority (68%) as solid phase, as expected due to precipitation of Fe(II) minerals (siderite and vivianite) during medium preparation (Hegler et al., 2008; Miot et al., 2009; Nordhoff et al., 2017; Tominski et al., 2018). Most importantly for the chemostat, as the medium was pumped in two days before inoculation, the absence of Fe(III) after 48 h provided confirmation that the chemostat was anoxic and could be used for cultivation of anoxic microorganisms. After a two-day lag phase after inoculation, rapid Fe(II) oxidation occurred. In the chemostat, no $Fe(II)_{aq}$ could be measured after day 3, even though fresh medium containing 2.8 mM $Fe(II)_{aq}$ was continuously pumped in, suggesting high microbial activity. At day 3, a low concentration of $Fe(II)_s$ (1.88 mM) was still measured, while at day 4 the $Fe(II)_s$ concentration decreased to 0.33 mM. This time delay between $Fe(II)_{aq}$ and $Fe(II)_s$ consumption implies that easily accessible $Fe(II)_{aq}$ was preferably oxidized. The absence of $Fe(II)_{aq}$ measured beyond day 4, despite continued addition, along with microscopy and nitrogen speciation data (discussed below), suggest microbial activity until the end of the experiment. The geochemical analyses of the chemostat were comparable to the results collected from the batch experiments (25 ml/700 ml - static/shaken). $Fe(II)_{aq}$ was quickly consumed (after 3 to 4 days) prior to $Fe(II)_s$ (4 to 5 days) and $Fe(II)_s$ (between 0.1 to 1 mM, see figures S4-S7) remained despite available $NO_3^-$ (concentrations of $Fe(II)_s$ at the end of experiments: 50 ml, static: 1 mM, 50 ml shaken: 0.3 mM, 700 ml static: 0.7 mM, 700 ml shaken: 0.56 mM, chemostat: 1 mM). These results agree with previous studies (Blöthe and Roden, 2009; Nordhoff et al., 2017; Tominski et al., 2018). We therefore hypothesize that culture KS

is not capable of fully oxidizing all solid-phase Fe(II). We were unable to identify this remaining Fe(II) mineral phase since neither μ-XRD nor Moessbauer measurements were conclusive. However, Tominski et al. (2018) described that culture KS was not capable of oxidizing vivianite, and thus, we suggest that such a Fe(II)-phosphate mineral could be the remaining $Fe(II)_s$. For the chemostat, Fe geochemistry data first suggested that steady state was reached at day 7, as we could only detect little $Fe(II)_s$ (0.2 mM) that seemed to be constant after day 4, and additionally no $Fe(II)_{aq}$ was measured. At day 14, however, more $Fe(II)_s$ was measured (1.24 mM), which suggests that the steady state was only achieved between days 7 to 14 in the chemostat (Figure 2). We suggest that at this time culture KS fully adapted to the conditions and quickly oxidized all bioavailable Fe(II) that was pumped into the chemostat. In all systems, the Fe(II) oxidation occurred simultaneously with $NO_3^-$ reduction, decreasing from approximately 4 mM to around 2 mM, and finally stabilizing at 2.2 mM for the chemostat. $NO_3^-$ reduction approached the expected extent based on the stoichiometric ratio of Fe to $NO_3^-$. Fe(II) oxidation yields 1 electron, reduction of $NO_3^-$ to $NO_2^-$ or $N_2$ requires 2 or 5 electrons, respectively. Therefore, a total of 10 mM Fe(II) (here the sum of $Fe(II)_{aq}$ and $Fe(II)_s$) could be oxidized by roughly 2 mM $NO_3^-$, with $N_2$ as product, as was shown by our data (Figure 2, Figures S4-S11). Averaged across all performed experiments (chemostat and all batch) 2.41 ± 0.28 mM of $NO_3^-$ was reduced. We propose an explanation for the surplus of reduced $NO_3^-$, even though some of the electrons from Fe oxidation must be used for $CO_2$ fixation: The uptake of electrons by Fe(II)-oxidizing bacteria can lead to an intracellular reduced redox environment (Guzman et al., 2019), suggesting that a surplus of electrons stored in the in pre-grown cells could explain the deviation from the expected ratio towards more $NO_3^-$ reduction. Interestingly, we detected approximately 15 μM of the reactive nitrogen species nitrite ($NO_2^-$) in the chemostat. Formation of nitrite has, to the best of our knowledge, not been previously reported for

275 culture KS. The detection of $NO_2^-$ occurred after the fastest rate of $NO_3^-$ reduction (between
276 day 3 and 6), when $NO_3^-$ was still being reduced. $NO_2^-$ is very reactive and will rapidly transform
277 to NO and $NO_2$, and react abiotically with Fe(II) to form $N_2O$ during chemodenitrification
278 (Dhakal et al., 2013; Klueglein and Kappler, 2013). We observed a slight delay between highest
279 $NO_3^-$ consumption and $NO_2^-$ formation of approximately 3 days. We propose that this shift is
280 caused by $NO_2^-$ consumption (biotically) and reactivity (chemodenitrification). All biotic batch
281 experiments showed a similar behaviour in terms of $NO_3^-$ reduction as well (Figures S8 - S11).
282 We detected $NO_2^-$ in the batch experiments, showing that it was not only produced in the
283 continuous system. The nitrite concentration was dependent on the experimental setup and
284 increased in the following order (mean values ± standard deviation): 50 ml static (12.5 ± 3.1
285 µM), 50 ml shaking (18.7 ± 6.2 µM), 700 ml shaking (37.5 ± 12.3 µM), 700 ml static (234 ±
286 102.4 µM) (Figures S8-S11). The highest concentration of $NO_2^-$ (234 µM) was detected in the
287 700-ml static bottles. We speculate that $NO_2^-$ was consumed more rapidly in the well mixed
288 systems and the systems of small volume, since there was no (agitation) or less diffusion
289 limitation of substrates (small volume). In the mixed setups, all compounds were
290 homogeneously distributed and hence geochemical gradients not expected, that could have
291 hindered microbial activity and abiotic reactivity between Fe(II) and $NO_2^-$, causing
292 accumulation of the latter.

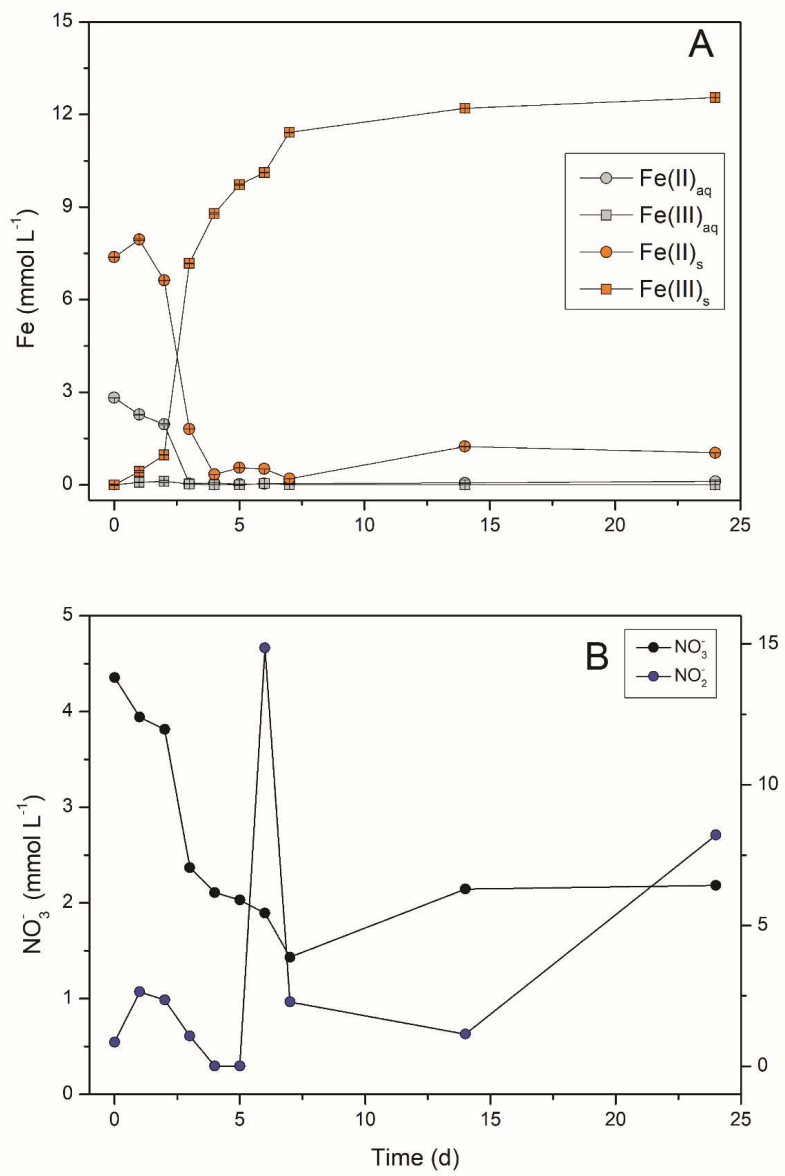


293 ***Figure 2.*** *Changes of Fe(II)/Fe(III) (A) and $NO_3^-$/$NO_2^-$ (B) concentrations in the chemostat during*
294 *autotrophic cultivation of culture KS for 25 days. Fe: Circles show Fe(II) species while squares*
295 *show Fe(III) species for aqueous (aq - blue) and solid phase (s - grey) iron (mmol $L^{-1}$). Error bars*
296 *represent measurement error (standard deviation) from ferrozine replicate measurements.*
297 *$NO_3^-$: black circles indicated $NO_3^-$ concentrations (mmol $L^{-1}$ - left y axis) while blue circles show*
298 *$NO_2^-$ concentrations (µmol $L^{-1}$ - right y axis).*

299 **Iron(II) oxidation rates in different cultivation conditions**

300 The calculated $Fe(II)_s$ oxidation rate was greater than the rate of oxidation for $Fe(II)_{aq}$ in all
301 setups. For the chemostat the $Fe(II)_{aq}$ oxidation rate was calculated at 2.36 mM $d^{-1}$ compared

to 5.21 mM $d^{-1}$ for $Fe(II)_s$ (see SI for detailed information). The total iron oxidation rate ($Fe(II)_{s+aq}$) in the chemostat was the highest, since Fe(II) was continuously provided. All calculated oxidation rates are listed in table 1. We applied an unpaired t-test to determine if there was any statistical significance in the differences between the treatments for which multiple replicates were available (no replicates were available for the chemostat). We observed a significant difference between the Fe(II) oxidation rates of solid and aqueous phases across all treatments (p=0.004). Furthermore, we observed a significant difference between the solid phase Fe(II) oxidation rate between different volumes (p=0.03), however no other treatments showed any significant differences (Table S2). We however stress that despite the difference of the oxidation rates of chemostat and batch experiments, significant differences cannot be inferred due to the lack of replicates.

| **Setup** | **Fe(II) oxidation (mM $d^{-1}$)** | |
|---|---|---|
| | *Aqueous Fe(II)* | *Solid phase Fe(II)* |
| 25 ml static | 1.95 ± 0.14 | 3.28 ± 1.38 |
| 25 ml shaken | 1.82 ± 0.39 | 4.35 ± 0.66 |
| 700 ml static | 2.57 ± 0.41 | 2.68 ± 1.11 |
| 700 ml shaken | 2.03 ± 0.51 | 2.99 ± 0.59 |
| Chemostat | 2.36 | 5.21 |

***Table 1.*** *Maximum iron oxidation rates calculated for aqueous iron(II) ($Fe(II)_{aq}$) and solid phase iron(II) ($Fe(II)_s$, for 25 ml and 700 ml batch experiments (static and shaken) and the chemostat. Errors correspond to 1 standard deviation (1σ) from the mean of biological replicates of the batch experiments. Biological replicates were not available for the chemostat so no error is reported.*

**Iron mineral formation and transformation**

$^{57}$Fe Moessbauer spectroscopy was used to follow changes of the oxidation state of solid Fe phases formed in the chemostat over time in addition to providing information about the mineral composition (Figure 3, Table S1). Results revealed that the inoculated starting sample was almost completely dominated by Fe(II), though the fit was incomplete without an Fe(III) doublet which accounted for 6.0% of the spectral area. The initial presence of a Fe(III) phase was caused by the inoculum, as culture KS was previously cultivated in Fe(II)-rich medium and transferred with oxidized Fe(III). The initial Fe(II) component most likely consists of a combination of siderite ($FeCO_3$) and vivianite ($Fe_3(PO_4)_2{\cdot}8(H_2O)$), which were expected to precipitate immediately after addition of dissolved $FeCl_2$ to the bicarbonate- and phosphate-containing medium, as discussed before. The precipitates in the chemostat were dominated by Fe(III) at day 3 (90.8% relative abundance) and the remaining 9.2% was Fe(II). A Fe(II) component of up to 18.3% relative abundance was still measured at day 14. This increase of spectral area of Fe(II) agrees with the increased concentration of Fe(II) measured with ferrozine assay for this timepoint. The final sample taken after 24 days was dominated by a superparamagnetic Fe(III) doublet with 94.9% spectral area. The remaining 5.1% corresponded to a Fe(II) doublet. The detected Fe(III) component is most likely a short range ordered Fe(III) (oxyhydr)oxide such as ferrihydrite, though without measuring the sample at lower temperature confirmation is not possible. Previous investigations of culture KS in batch systems have revealed similar mineral formation products to those reported in this study, i.e. (short range ordered) ferrihydrite (Nordhoff et al., 2017). These similarities suggest, unexpectedly, that the stirring and continuity of the chemostat does not lead to major differences in mineral precipitation despite having the highest total oxidation rate. The Fe(II) phase could resemble vivianite, as suggested by previous reports, but this could not be

confirmed without further measurements. Oxidized Fe(III) minerals continuously accumulated in the chemostat bioreactor up to concentrations of 12.5 mM, higher than the concentration of the added medium (10 mM total Fe) (Figure 2). This increase was caused by Fe(III) (oxyhydr)oxide settling to the bottom of the reactor throughout the 24 day experiment during the gentle agitation (50 rpm). Additionally, the tubing for liquid removal was placed just below the surface of the medium, as settling of Fe(III) led to clogging of tubing in numerous test runs. The Fe(III) phases accumulated at the bottom of the vessel and we consequently anticipate that given even longer incubation time, continued addition of medium, and microbial activity, other minerals of higher crystallinity such as goethite or lepidocrocite may form (Hansel et al., 2003; Han et al., 2020). μ-XRD patterns (Figure S12) of samples indicated the presence of crystalline mineral reflections (2θ of 36° and 53°) in all samples which most likely correspond to dried salts from the medium as well as reflections from the sample holder (2θ of 52° and 65°). The only Fe mineral detected in any of the samples was found in a sample collected from the chemostat at day 14, with reflections most closely matching vivianite (Fig s12 - c), which was to be expected as previously described. The absence of any other reflections corresponding to Fe minerals, despite the clear abundance of solid Fe in each sample, suggests the presence of a short-range ordered Fe mineral such as ferrihydrite, which does not typically yield a clear diffraction pattern with the X-ray source used here (see samples 25 ml shaken (fig s12 - a), and 700 ml shaken (fig s12 - b)). The diffractogram of the chemostat sample collected after 24 days (fig s12 - d) exhibited reflections which most closely match being wuestite. However, the presence of this mineral is unlikely because wuestite is typically found in more reducing conditions (Cornell and Schwertmann, 2003) or at higher temperatures (Jette and Foote, 1933). This additional reflection of sample taken from the chemostat at 24 days (fig s12 – d) however shows that more crystalline phases are forming over time, further confirmed by

XAS measurements. After the final sampling of the experiment, the chemostat was still maintained continuously for another 20 days. At day 40, a sample of the very bottom of the bioreactor vessel was taken and prepared for XAS measurements. The results (Figures S13 and S14) showed crystalline Fe(III) phases: 48.7 mole% goethite and 11.6 mole% lepidocrocite. Still, around 40 mole% of detected Fe(III) phases were determined to be ferrihydrite in this sample. Ferrihydrite is the primary initial product of Fe(II) oxidation by culture KS as previously shown (Nordhoff et al., 2017; Tominski et al., 2018). The presence of more crystalline phases confirms mineral transformation over time in the chemostat. Previous studies have shown that low concentrations of Fe(II) can cause transformation to lepidocrocite and goethite (Hansel et al., 2005). Hence a mineral transformation is likely. Since we continuously added Fe(II) to the chemostat, and also measured some leftover $Fe(II)_s$ (after 24 days) we suggest transformation to a greater extent in the chemostat than in the batch systems.

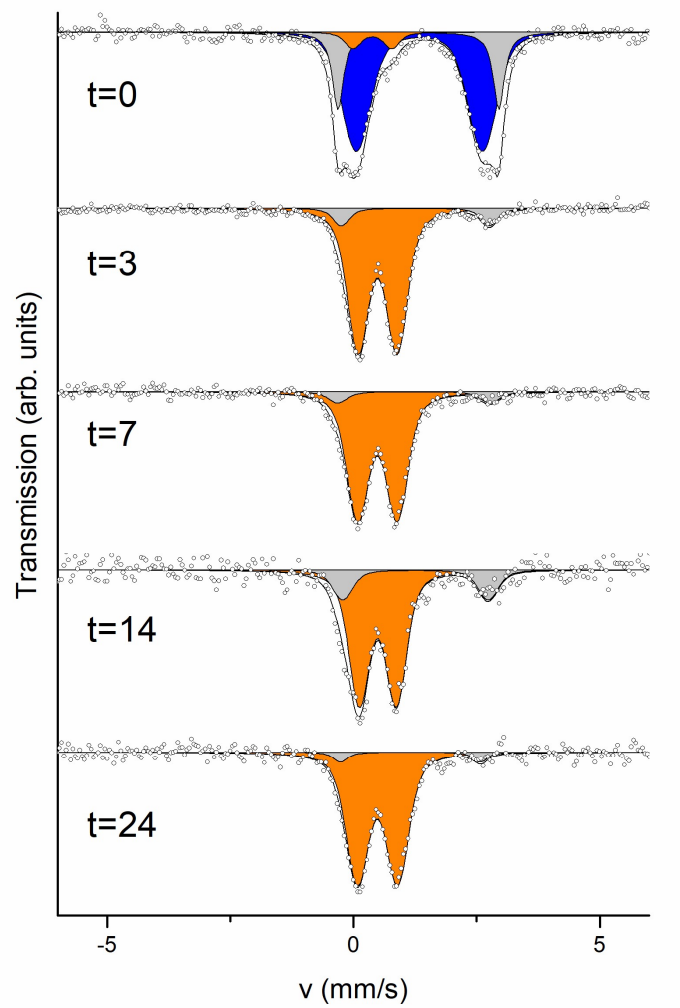


***Figure 3.*** *$^{57}$Fe Moessbauer spectra of anoxically filtered mineral precipitates formed in the chemostat during autotrophic NRFeOx by culture KS (collected after 0, 3, 7, 14, and 24 days of continuous cultivation in the chemostat).*

**Cell encrustation during autotrophic NRFeOx visualized by SEM**

The interaction between Fe minerals and cells from culture KS were visualized using SEM (Figure 4), focusing mainly on the chemostat, after confirming that cells had the same morphology and showed the same encrustation patterns for all experiments. The micrographs revealed that many cells were associated with Fe minerals to varying degrees (Figure S15). Of all imaged cells (n = 78), 58% were free of iron minerals, 31% were closely associated/partly encrusted with iron minerals, and 11% were completely encrusted with Fe minerals. Based on the morphology of the cells, it is likely that these cells are *Gallionellaceae* sp. (Nordhoff et al.,

2017). This is also supported by previous work, where *Gallionellaceae* sp. was reported as the dominating species enrichment culture when grown autotrophically (Tominski et al., 2018). Until now, the absence of encrustation by culture KS, alongside with the lack of detection of $NO_2^-$, were used to support the hypothesis of exclusively enzymatic Fe(II) oxidation (Straub et al., 1996; Nordhoff et al., 2017; Tominski et al., 2018). In contrast to this, we show that 42% of all imaged cells were at least partly associated with minerals and that 11% were completely encrusted, and therefore suggest that not all oxidation is enzymatic. Since we quantified $NO_2^-$ (Fig.2 and S8-S10) and saw 42% of all counted cells to be at least slightly encrusted, abiotic oxidation of Fe(II) (chemodenitrification) should be considered during autotrophic NRFeOx by culture KS. These findings suggest that future research needs to account for these processes when studying NRFeOx, especially when calculating turnover rates of Fe(II) and $NO_3^-/NO_2^-$. In cultures of the NRFeOx *Acidovorax sp*. BoFeN1, encrustation by Fe(III) mineral precipitates was shown to occur as a result of abiotic Fe(II) oxidation by $NO_2^-$ (Klueglein and Kappler, 2013; Klueglein et al., 2014; Schmid et al., 2014). We suggest that this abiotic oxidation due to $NO_2^-$ or NO also occurred in in this study. The main Fe(II)-oxidizer of culture KS, *Gallionellaceae* sp., is suggested to be unable to perform NO-reduction enzymatically and hence relies on other members of the enrichment culture to perform NO-detoxification (He et al., 2016; Huang et al., 2021a). Prolonged presence of NO, and possibly $NO_2^-$, could have caused the encrustation, which could have limited access to substrates as well as interfere with cell growth and division. We speculate that the extent of encrustation varies depending on the age of individual cells, the amount of RNS produced, and the abundance of flanking community members, which are essential for RNS-removal. Additionally, intact surface areas of dead cells could serve as a template for mineral-precipitation similar to the way that twisted stalk forming Fe(II)-oxidizing bacteria provide a template for mineral precipitation (Chan et al., 2011). This dead-cell-

encrustation would, however, limit organic compounds from dead cells, that would otherwise be available from lysed cells. If this process is happening in anoxic, $NO_3^-$-rich aquatic systems, where Fe(II) is oxidized, cell encrustation would effectively trap organic carbon (cells and content) within this system. In the chemostat, even after 24 days of continuous cultivation, geochemical measurements, fluorescence microscopy (figure S16) and SEM micrographs (figure 4) suggested viable cells. We therefore propose that the chemostat bioreactors' design fulfils the requirements to study NRFeOx over extended periods of time.

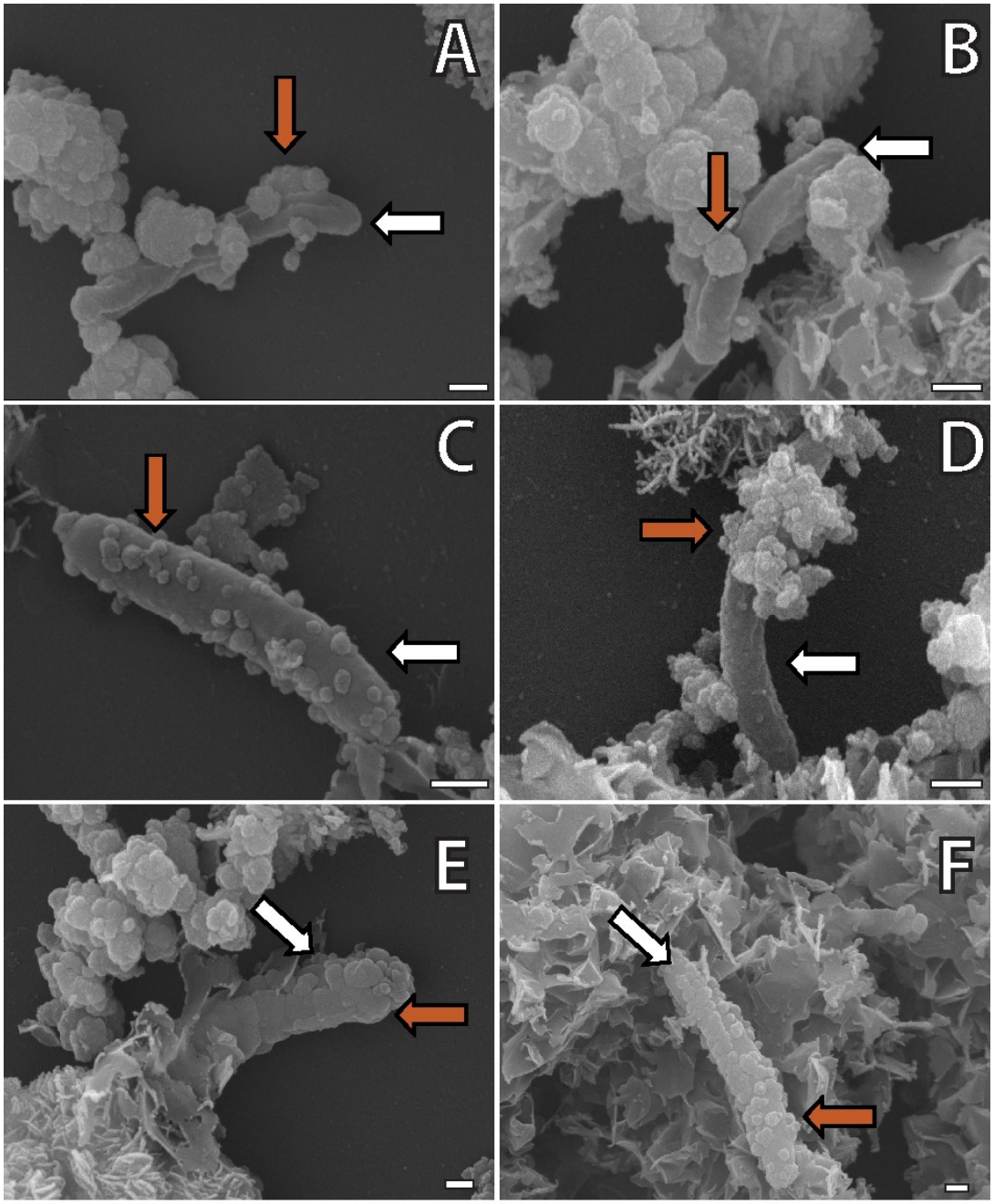

***Figure 4.*** *Scanning electron micrographs of culture KS grown autotrophically in the chemostat under continuous cultivation. Micrographs were collected at 15 kV acceleration voltage. A, B and C: Cells that are associated to a small extent with minerals. D, E and F: Cells that become encrusted with iron minerals. White scale bar represents 200 nm. White arrows indicate not encrusted cell surface and orange arrows point to different degrees of encrustation*

**Advantages and challenges of continuous cultivation in a chemostat**

The majority of experiments that have focused on anaerobic microbial Fe(II) oxidation were carried out in small-volume (commonly <100 ml) batch systems. This approach is long established and works well, but limits the ability to better understand more complex environmental settings and possibly obfuscates more complex reaction mechanisms and processes, for which substrate availability may be steadier, mixing may occur, or volumes and time scales might be significantly larger. Also, introduction of sampling artefacts due to removal of too much volume are a great concern, confining the amount of sample that should be removed, and hence applied methods. To circumvent these limitations, we established a chemostat for continuous cultivation of Fe(II)-oxidizing bacteria, here for the autotrophic NRFeOx culture KS. Compared to our experimental control setups, which represent more conventional batch cultivation methods, and previously published data (Nordhoff et al., 2017; Tominski et al., 2018), the chemostat showed comparable results for Fe(II) oxidation rates and Fe mineralogy. Compared to our performed batch experiments, the total rate Fe(II) oxidation was highest in the chemostat, as metabolising cells were provided with a continuous supply of Fe(II). This suggests the successful establishment of this anoxic incubation bioreactor to cultivate anaerobic microbes over long time periods in well mixed steady state conditions. Additionally, we showed mineral transformation over time during continuous cultivation of KS in the chemostat. Ostwald ripening is a well described process for minerals and time-

dependent ripening of ferrihydrite to more crystalline phases like goethite and Fe(II) catalysed transformations were previously described (Cornell and Schwertmann, 2003; Burleson and Penn, 2006; Tomaszewski et al., 2017). This could have great influence for long term experiments, as mineral surfaces greatly influence nutrient availability (Gu et al., 1994) and heterogeneous Fe(II) oxidation (Sørensen and Thorling, 1991; Hansen et al., 1994). Maintaining $O_2$-free conditions despite connecting multiple tubes which could have been points of failure (Figure S1) was achieved by applying a slight overpressure and proper attachment and sealing of all connections. High mixing velocities needed to be avoided to ensure cell viability while homogenizing the volume as well as possible. Chemostats are built for long term experiments, and hence performing several replicated runs for extended periods of time is challenging, as setting up takes significantly more time than batch experiments and is prone to difficulties. Additionally, parallel setups are only possible with multiple chemostats. Lack of replicates is an obvious disadvantage compared to the smaller batch setups, where multiple replicates can be easily performed in parallel. Key aspects that should be considered when working anoxically and under sterile conditions with the chemostat are: 1) sterilization and sterile connection of large vessels, 2) sterile addition of anoxic medium and inoculum of bacteria, and 3) maintaining anoxic conditions during long-term cultivation and sampling. Further details are described in the supplementary information. The chemostat setup presented here was optimized for the cultivation of enrichment culture KS. We suggest it could be applied for different types of Fe(II)-oxidizing bacteria. However, predicting behaviour of bacteria in a new cultivation vessel is uncertain, and hence we suggest performing all controls as described here. Despite these challenges and the limited replication possibilities, the chemostat bioreactor is a valuable tool to investigate microbial activity under continuous conditions.

## Conclusion

We have successfully established a chemostat bioreactor system for investigating NRFeOx. By using it, we have for the first time measured the RNS $NO_2^-$ in autotrophic culture KS. $NO_2^-$ can abiotically oxidize Fe(II), possibly influencing rates and competing with the enzymatic oxidation of Fe(II) by culture KS. We therefore suggest that chemodenitrification should be considered even during autotrophic NRFeOx. For future studies, we propose to carefully follow $NO_2^-$, NO, and $N_2O$ formation when studying NRFeOx, for a better understanding of production and impact on Fe(II) oxidation of RNS like $NO_2^-$ and NO. We used SEM to show different associations of cells with Fe minerals, including complete cell encrustation. We propose that encrustation might be promoted by abiotic oxidation of Fe(II) due to $NO_2^-$. Geochemical data collected during growth of culture KS in the chemostat showed that we successfully established an anoxic and sterile growth reactor to study NRFeOx under continuous conditions. We showed microbial activity for at least 24 days, allowing us to better understand processes that could be happening in a continuous and anoxic environment, that these microbes could be inhabiting in nature. Iron oxidation rates calculated for the chemostat were in the same order of magnitude compared to batch studies. The chemostat however showed the highest total oxidation rate. We focused on NRFeOx culture KS, though the chemostat system can be adapted to phototrophic Fe(II)-oxidizers by providing a light source as well as for microaerophilic Fe(II)-oxidizers by bubbling a defined gas mixture into the system. Overall, the chemostat provides a powerful tool in studying Fe(II)-oxidizing microorganisms in continuous cultivation with constant supply of nutrients and substrates, which allows studying microbial activity for a prolonged time and allowed to detect so far undescribed processes of nitrite formation and cell encrustation for chemolithoautotrophic culture KS.

**Acknowledgements**

The authors thank Natalia Jakus for µ-XRD measurements and help with sample analysis. Markus Turad and Ronny Löffler (LISA$^+$, University of Tübingen) for access to and help with scanning electron microscopy as well as Hartmut Schulz for help with scanning electron microscopy. Julian Sorwat and Manuel Schad for Moessbauer measurements. Lars Grimm for help with cultivation of culture KS. The authors acknowledge APS for XAS measurements: MRCAT operations are supported by the Department of Energy and the MRCAT member institutions. This research used resources of the Advanced Photon Source, a U.S. Department of Energy (DOE) Office of Science User Facility operated for the DOE Office of Science by Argonne National Laboratory under Contract No. DE-AC02-06CH11357. The authors acknowledge funding from Deutsche Forschungsgemeinschaft (DFG, German Research Foundation; BY 82/2-1) awarded to J. M. Byrne as well as infrastructural support by the DFG under Germany's Excellence Strategy, cluster of Excellence EXC2124, project ID 390838134.

## Supporting information

Detailed description of the setup of the chemostat, additional tables and figures, and logged data of the chemostat are included in the SI.

## Conflict of interest

The authors declare no conflict of interest.

# 1 References


Benz, M., Brune, A., and Schink, B. (1998) Anaerobic and aerobic oxidation of ferrous iron at neutral pH by chemoheterotrophic nitrate-reducing bacteria. *Arch of Microbiol* **169**: 159-165.

Betlach, M.R., and Tiedje, J.M. (1981) Kinetic explanation for accumulation of nitrite, nitric oxide, and nitrous oxide during bacterial denitrification. *Appl Environ Microbiol* **42**: 1074-1084.

Blöthe, M., and Roden, E.E. (2009) Composition and activity of an autotrophic Fe (II)-oxidizing, nitrate-reducing enrichment culture. *Appl Environ Microbiol* **75**: 6937-6940.

Borch, T., Kretzschmar, R., Kappler, A., Cappellen, P.V., Ginder-Vogel, M., Voegelin, A., and Campbell, K. (2009) Biogeochemical redox processes and their impact on contaminant dynamics. *Environ Sci Technol* **44**: 15-23.

Boyd, P., and Ellwood, M. (2010) The biogeochemical cycle of iron in the ocean. *Nature Geosci* **3**: 675.

Bryce, C., Blackwell, N., Schmidt, C., Otte, J., Huang, Y.M., Kleindienst, S. et al. (2018) Microbial anaerobic Fe(II) oxidation–Ecology, mechanisms and environmental implications. *Env Microbiol* **20**: 3462-3483.

Burleson, D.J., and Penn, R.L. (2006) Two-Step Growth of Goethite from Ferrihydrite. *Langmuir* **22**: 402-409.

Canfield, D.E., Glazer, A.N., and Falkowski, P.G. (2010) The evolution and future of Earth's nitrogen cycle. *Science* **330**: 192-196.

Chan, C.S., Fakra, S.C., Emerson, D., Fleming, E.J., and Edwards, K.J. (2011) Lithotrophic iron-oxidizing bacteria produce organic stalks to control mineral growth: implications for biosignature formation. *The ISME J* **5**: 717-727.

Coby, A.J., Picardal, F., Shelobolina, E., Xu, H., and Roden, E.E. (2011) Repeated anaerobic microbial redox cycling of iron. *Appl Environ Microbiol* **77**: 6036-6042.

Cornell, R.M., and Schwertmann, U. (2003) *The iron oxides: structure, properties, reactions, occurrences and uses*: John Wiley & Sons.

Daugherty, E.E., Gilbert, B., Nico, P.S., and Borch, T. (2017) Complexation and Redox Buffering of Iron(II) by Dissolved Organic Matter. *Environ Sci Technol* **51**: 11096-11104.

Dhakal, P., Matocha, C., Huggins, F., and Vandiviere, M. (2013) Nitrite reactivity with magnetite. *Environ Sci Technol* **47**: 6206-6213.

Druschel, G.K., Emerson, D., Sutka, R., Suchecki, P., and Luther III, G.W. (2008) Low-oxygen and chemical kinetic constraints on the geochemical niche of neutrophilic iron(II) oxidizing microorganisms. *Geochim Cosmochim Acta* **72**: 3358-3370.

Ehrenreich, A., and Widdel, F. (1994) Anaerobic oxidation of ferrous iron by purple bacteria, a new type of phototrophic metabolism. *Appl Environ Microbiol* **60**: 4517-4526.

Emerson, D., and Moyer, C. (1997) Isolation and characterization of novel iron-oxidizing bacteria that grow at circumneutral pH. *Appl Environ Microbiol* **63**: 4784-4792.

Emmerich, M., Bhansali, A., Lösekann-Behrens, T., Schröder, C., Kappler, A., and Behrens, S. (2012) Abundance, distribution, and activity of Fe(II)-oxidizing and Fe(III)-reducing microorganisms in hypersaline sediments of Lake Kasin, southern Russia. *Appl Environ Microbiol* **78**: 4386-4399.

Finneran, K.T., Housewright, M.E., and Lovley, D.R. (2002) Multiple influences of nitrate on uranium solubility during bioremediation of uranium-contaminated subsurface sediments. *Env Microbiol* **4**: 510-516.

Gu, B., Schmitt, J., Chen, Z., Liang, L., and McCarthy, J.F. (1994) Adsorption and desorption of natural organic matter on iron oxide: mechanisms and models. *Environ Sci Technol* **28**: 38-46.

Guzman, M.S., Rengasamy, K., Binkley, M.M., Jones, C., Ranaivoarisoa, T.O., Singh, R. et al. (2019) Phototrophic extracellular electron uptake is linked to carbon dioxide fixation in the bacterium Rhodopseudomonas palustris. *Nature Commun* **10**: 1355.

Hafenbradl, D., Keller, M., Dirmeier, R., Rachel, R., Roßnagel, P., Burggraf, S. et al. (1996) Ferroglobus placidus gen. nov., sp. nov., a novel hyperthermophilic archaeum that oxidizes Fe2+ at neutral pH under anoxic conditions. *Arch Microbiol* **166**: 308-314.

Han, X., Tomaszewski, E.J., Sorwat, J., Pan, Y., Kappler, A., and Byrne, J.M. (2020) Effect of Microbial Biomass and Humic Acids on Abiotic and Biotic Magnetite Formation. *Environ Sci Technol* **54**: 4121-4130.

Hansel, C.M., Benner, S.G., and Fendorf, S. (2005) Competing Fe(II)-induced mineralization pathways of ferrihydrite. *Environ Sci Technol* **39**: 7147-7153.

Hansel, C.M., Benner, S.G., Neiss, J., Dohnalkova, A., Kukkadapu, R.K., and Fendorf, S. (2003) Secondary mineralization pathways induced by dissimilatory iron reduction of ferrihydrite under advective flow. *Geochim Cosmochim Acta* **67**: 2977-2992.

Hansen, H.C.B., Borggaard, O.K., and Sørensen, J. (1994) Evaluation of the free energy of formation of Fe(II)-Fe(III) hydroxide-sulphate (green rust) and its reduction of nitrite. *Geochim Cosmochim Acta* **58**: 2599-2608.

He, S., Tominski, C., Kappler, A., Behrens, S., and Roden, E.E. (2016) Metagenomic Analyses of the Autotrophic Fe(II)-Oxidizing, Nitrate-Reducing Enrichment Culture KS. *Appl Environ Microbiol* **82**: 2656-2668.

Hedrich, S., Schlömann, M., and Johnson, D.B. (2011) The iron-oxidizing proteobacteria. *Microbiol* **157**: 1551-1564.

Hegler, F., Posth, N.R., Jiang, J., and Kappler, A. (2008) Physiology of phototrophic iron (II)-oxidizing bacteria: implications for modern and ancient environments. *FEMS Microbiol Ecol* **66**: 250-260.

Huang, Y.M., Straub, D., Blackwell, N., Kappler, A., and Kleindienst, S. (2021a) Meta-omics Reveal Gallionellaceae and Rhodanobacter Species as Interdependent Key Players for Fe(II) Oxidation and Nitrate Reduction in the Autotrophic Enrichment Culture KS. *Appl Environ Microbiol* **87**: e0049621.

Huang, Y.M., Straub, D., Kappler, A., Smith, N., Blackwell, N., and Kleindienst, S. (2021b) A Novel Enrichment Culture Highlights Core Features of Microbial Networks Contributing to Autotrophic Fe(II) Oxidation Coupled to Nitrate Reduction. *Microb Physio* **31**: 280-295.

Jakus, N., Mellage, A., Hoeschen, C., Maisch, M., Byrne, J.M., Mueller, C.W. et al. (2021a) Anaerobic neutrophilic pyrite oxidation by a chemolithoautotrophic nitrate-reducing iron(II)-oxidizing culture enriched from a fractured aquifer. *Environ Sci Technol* **55**: 9876-9884.

Jakus, N., Blackwell, N., Osenbruck, K., Straub, D., Byrne, J.M., Wang, Z. et al. (2021b) Nitrate Removal by a Novel Lithoautotrophic Nitrate-Reducing, Iron(II)-Oxidizing Culture Enriched from a Pyrite-Rich Limestone Aquifer. *Appl Environ Microbiol* **87**: e0046021.

Jette, E.R., and Foote, F. (1933) An X-Ray Study of the Wüstite (FeO) Solid Solutions. *The J of Chem Phys* **1**: 29-36.

Kampschreur, M.J., Kleerebezem, R., de Vet, W.W., and van Loosdrecht, M.C. (2011) Reduced iron induced nitric oxide and nitrous oxide emission. *Water Res* **45**: 5945-5952.

Kappler, A., Schink, B., and Newman, D.K. (2005) Fe(III) mineral formation and cell encrustation by the nitrate-dependent Fe(II)-oxidizer strain BoFeN1. *Geobiol* **3**: 235-245.

Kappler, A., Becker, S., and Enright, A.M.L. (2021a) Metals, Microbes, and Minerals - The Biogeochemical Side of Life. In *Living On Iron*. Peter, K., and Martha Sosa, T. (eds): De Gruyter, pp. 185-228.

Kappler, A., Bryce, C., Mansor, M., Lueder, U., Byrne, J.M., and Swanner, E.D. (2021b) An evolving view on biogeochemical cycling of iron. *Nature Rev Microbiol* **19**: 360-374.

Kendall, B., Anbar, A.D., Kappler, A., and Konhauser, K.O. (2012) The global iron cycle. *Fundame of Geobiol* **1**: 65-92.

Kim, H., Kaown, D., Mayer, B., Lee, J.-Y., Hyun, Y., and Lee, K.-K. (2015) Identifying the sources of nitrate contamination of groundwater in an agricultural area (Haean basin, Korea) using isotope and microbial community analyses. *Sci of the tot Environ* **533**: 566-575.

Klueglein, N., and Kappler, A. (2013) Abiotic oxidation of Fe(II) by reactive nitrogen species in cultures of the nitrate-reducing Fe(II) oxidizer Acidovorax sp. BoFeN1 - questioning the existence of enzymatic Fe(II) oxidation. *Geobiol* **11**: 180-190.

Klueglein, N., Zeitvogel, F., Stierhof, Y.D., Floetenmeyer, M., Konhauser, K.O., Kappler, A., and Obst, M. (2014) Potential role of nitrite for abiotic Fe(II) oxidation and cell encrustation during nitrate reduction by denitrifying bacteria. *Appl Environ Microbiol* **80**: 1051-1061.

Laufer, K., Byrne, J.M., Glombitza, C., Schmidt, C., Jørgensen, B.B., and Kappler, A. (2016) Anaerobic microbial Fe(II) oxidation and Fe(III) reduction in coastal marine sediments controlled by organic carbon content. *Env Microbiol* **18**: 3159-3174.

Liu, T., Chen, D., Li, X., and Li, F. (2019a) Microbially mediated coupling of nitrate reduction and Fe(II) oxidation under anoxic conditions. *FEMS Microbiol Ecol* **95**: fiz030.

Liu, T., Chen, D., Luo, X., Li, X., and Li, F. (2019b) Microbially mediated nitrate-reducing Fe(II) oxidation: Quantification of chemodenitrification and biological reactions. *Geochim Cosmochim Acta* **256**: 97-115.

Maisch, M., Lueder, U., Laufer, K., Scholze, C., Kappler, A., and Schmidt, C. (2019) Contribution of microaerophilic iron(II)-oxidizers to iron(III) mineral formation. *Environ Sci Technol* **53**: 8197-8204.

Melton, E.D., Schmidt, C., and Kappler, A. (2012) Microbial iron(II) oxidation in littoral freshwater lake sediment: the potential for competition between phototrophic vs. nitrate-reducing iron(II)-oxidizers. *Fron Microbiol* **3**: 197.

Miot, J., Benzerara, K., Morin, G., Bernard, S., Beyssac, O., Larquet, E. et al. (2009) Transformation of vivianite by anaerobic nitrate-reducing iron-oxidizing bacteria. *Geobiol* **7**: 373-384.

Muehe, E.M., Gerhardt, S., Schink, B., and Kappler, A. (2009) Ecophysiology and the energetic benefit of mixotrophic Fe(II) oxidation by various strains of nitrate-reducing bacteria. *FEMS Microbiol Ecol* **70**: 335-343.

Nordhoff, M., Tominski, C., Halama, M., Byrne, J.M., Obst, M., Kleindienst, S. et al. (2017) Insights into nitrate-reducing Fe(II) oxidation mechanisms through analysis of cell-mineral associations, cell encrustation, and mineralogy in the chemolithoautotrophic enrichment culture KS. *Appl Environ Microbiol* **83**: e00752-00717.

637 Peiffer, S., Kappler, A., Haderlein, S.B., Schmidt, C., Byrne, J.M., Kleindienst, S. et al. (2021) A
638 biogeochemical–hydrological framework for the role of redox-active compounds in aquatic systems.
639 *Nature Geosci* **14**: 264-272.

640 Roden, Eric E. (2012) Microbial iron-redox cycling in subsurface environments. *Biochemical Society*
641 *Transactions* **40**: 1249-1256.

642 Schaedler, F., Kappler, A., and Schmidt, C. (2017) A Revised Iron Extraction Protocol for Environmental
643 Samples Rich in Nitrite and Carbonate. *Geomicrobiol J* **35**: 23-30.

644 Schmid, G., Zeitvogel, F., Hao, L., Ingino, P., Floetenmeyer, M., Stierhof, Y.-D. et al. (2014) 3-D analysis
645 of bacterial cell-(iron)mineral aggregates formed during Fe(II) oxidation by the nitrate-reducing
646 Acidovorax sp. strain BoFeN1 using complementary microscopy tomography approaches. *Geobiol* **12**:
647 340-361.

648 Segre, C., Leyarovska, N., Chapman, L., Lavender, W., Plag, P., King, A. et al. (2000) The MRCAT insertion
649 device beamline at the Advanced Photon Source. In *AIP Conference Proceedings*: American Institute of
650 Physics, pp. 419-422.

651 Shimizu, M., Zhou, J., Schröder, C., Obst, M., Kappler, A., and Borch, T. (2013) Dissimilatory Reduction
652 and Transformation of Ferrihydrite-Humic Acid Coprecipitates. *Environ Sci Technol* **47**: 13375-13384.

653 Sørensen, J., and Thorling, L. (1991) Stimulation by lepidocrocite (7-FeOOH) of Fe(II)-dependent nitrite
654 reduction. *Geochim Cosmochim Acta* **55**: 1289-1294.

655 Stookey, L.L. (1970) Ferrozine - a new spectrophotometric reagent for iron. *Anal Chem* **42**: 779-781.

656 Straub, K.L., Hanzlik, M., and Buchholz-Cleven, B.E. (1998) The use of biologically produced ferrihydrite
657 for the isolation of novel iron-reducing bacteria. *System and Appl Microbiol* **21**: 442-449.

658 Straub, K.L., Benz, M., Schink, B., and Widdel, F. (1996) Anaerobic, nitrate-dependent microbial
659 oxidation of ferrous iron. *Appl Environ Microbiol* **62**: 1458-1460.

660 Swanner, E.D., Mloszewska, A.M., Cirpka, O.A., Schoenberg, R., Konhauser, Kurt O., and Kappler, A.
661 (2015) Modulation of oxygen production in Archaean oceans by episodes of Fe(II) toxicity. *Nature*
662 *Geosci* **8**: 126-130.

663 Tiedje, J.M. (1988) Ecology of denitrification and dissimilatory nitrate reduction to ammonium. *Biology*
664 *of anaerobic microorganisms* **717**: 179-244.

665 Tomaszewski, E.J., Lee, S., Rudolph, J., Xu, H., and Ginder-Vogel, M. (2017) The reactivity of Fe(II)
666 associated with goethite formed during short redox cycles toward Cr(VI) reduction under oxic
667 conditions. *Chem Geol* **464**: 101-109.

668 Tominski, C., Heyer, H., Lösekann-Behrens, T., Behrens, S., and Kappler, A. (2018) Growth and
669 population dynamics of the anaerobic Fe(II)-oxidizing and nitrate-reducing enrichment culture KS. *Appl*
670 *Environ Microbiol* **84**: e02173-02117.

671 Visser, A.-N., Lehmann, M.F., Rügner, H., D'Affonseca, F.M., Grathwohl, P., Blackwell, N. et al. (2021)
672 Fate of nitrate during groundwater recharge in a fractured karst aquifer in Southwest Germany.
673 *Hydrogeol J* **29**: 1153-1171.

674 Ward, M.H., Jones, R.R., Brender, J.D., De Kok, T.M., Weyer, P.J., Nolan, B.T. et al. (2018) Drinking water
675 nitrate and human health: an updated review. *International journal of environmental research and*
676 *public health* **15**: 1557.

677 Weber, K.A., Urrutia, M.M., Churchill, P.F., Kukkadapu, R.K., and Roden, E.E. (2006) Anaerobic redox
678 cycling of iron by freshwater sediment microorganisms. *Env Microbiol* **8**: 100-113.

679 Weusthuis, R.A., Pronk, J.T., Van Den Broek, P., and Van Dijken, J. (1994) Chemostat cultivation as a
680 tool for studies on sugar transport in yeasts. *Microbiol rev* **58**: 616-630.

681 Widdel, F., Schnell, S., Heising, S., Ehrenreich, A., Assmus, B., and Schink, B. (1993) Ferrous iron
682 oxidation by anoxygenic phototrophic bacteria. *Nature* **362**: 834.

683

684

685 **Supplementary information**

686

687 **Chemostat setup**

688 The chemostat used in this study (see reaction vessel in Fig. 1) was model
689 BioFlo®/CelliGen®115, Benchtop Fermentor & Bioreactor (New Brunswick, an Eppendorf
690 company). Manual No: M1369-0050, Revision B, June 2, 2009 (New Brunswick Scientific,
691 Edison, USA; software BF115 Rev B). It consists of a reaction chamber and a control unit. All
692 metal surfaces are 316L or 316 stainless steel. Separate parts included:

693 1) The reaction vessel, made from borosilicate glass, total volume of approximately 1 L.
694 The reaction chamber is sealed airtight with a stainless-steel head plate with ten
695 openings. The reaction chamber is tightly closed with a rubber seal. The reaction
696 chamber can be enveloped in a Peltier-element-type heating vest, for maintaining a
697 constant temperature. The chamber is attached to a four-footed stainless-steel holder.
698 2) The control unit, equipped with a touchscreen and various connection ports, allows
699 following and adjusting pH, dissolved oxygen concentration (DO), temperature (T),
700 water level and agitation.

701 Unless denoted otherwise, all connections for gas and medium exchange consist of stainless-
702 steel capillaries (I/16" outer diameter, 1.0 mm inner diameter, ref. number 7.590133
703 CH.211661, Ziemer Chromatography; Klaus Ziemer GmbH, Langerwehe, Germany). Two types
704 of tubing were used to enable pumping with peristaltic pumps. For external pumps, black
705 pumping tubing (ID: 0.74 mm, wall: 0.91 mm, reference 070652 – 07i / SC0257, IDEX, Health
706 & Science, ISMATEC®, Wertheim, Germany) was used. For the built-in pumps, yellow pumping
707 tubing were used (Flexible Plastic Tubing, ID: 0.8 mm, OD: 4.0 mm, wall: 1.6 mm, PharMed® -

BPT, Saint-Gobain Performance Plastics, Charny, France). External pumps were set to continuously pump medium in and out of the reaction vessel. Pumping in rate (15 ml $h^{-1}$) was greater than pumping out (8 ml $h^{-1}$) to ensure constant volume. Using the controller units' *loops* option an additional pump was set to start at approximately 710 ml and reduced the volume back to 700 ml.

All sensors were attached using mounting threads, sealed with a Teflon and rubber ring, and additionally sealed with a Teflon thin foil (Maagtechnic, 60 g/$m^2$, BAM Tgb. EN751-3 FRp) on the inside of all threads. All other ports were sealed using rubber stoppers. The system was continuously flushed with an overpressure of about 10 mbar $N_2/CO_2$ (90:10, v/v). $N_2/CO_2$ was supplied from an external gas bottle (UN 1956, verdichtetes Gas, N.A.G., Westfalen AG, Münster, Germany. To maintain sterile conditions, the gas was fed through a cotton filled glass syringe, that was previously oven-sterilized (180°C, 4.5 h). This glass syringe was connected to a gas splitter made of stainless steel with a *Luer-lock* system. All air flow was led to a Schott bottle filled with sterilized, anoxic water. Here, all pressure will accumulate and gradually escape. To ensure that there is an actual gas flow, bubbles of outgassing air could be seen in the bottle ("*pressure valve*").

To enable continuous supply of bacterial growth medium to the system, Schott bottles with a volume of 2 L were chosen. Gas entered the medium bottle from the gas-splitter and then led to i) the chemostat and ii) the waste bottle.

After sterilization of the chemostats' reaction chamber and attaching the gas flow, the mixing motor was set to 200 rpm to purge oxygen from the system. The sterilized, polarized and calibrated dissolved oxygen (DO) sensor was attached.

A 2 L Schott bottle was connected for outflow collection before autoclaving and was not removed unless it was filled up. In that case, the bottle was replaced with another sterilized, degassed 2 L Schott bottle. Gas flow to this waste bottle was connected from the medium supply and the reaction vessel. Pumping from top and bottom layers of the reaction vessel were also fed into this bottle. A single capillary was connected to the previously mentioned *pressure-valve* bottle.

736

737 **Figure S1:** Overview of the chemostat.

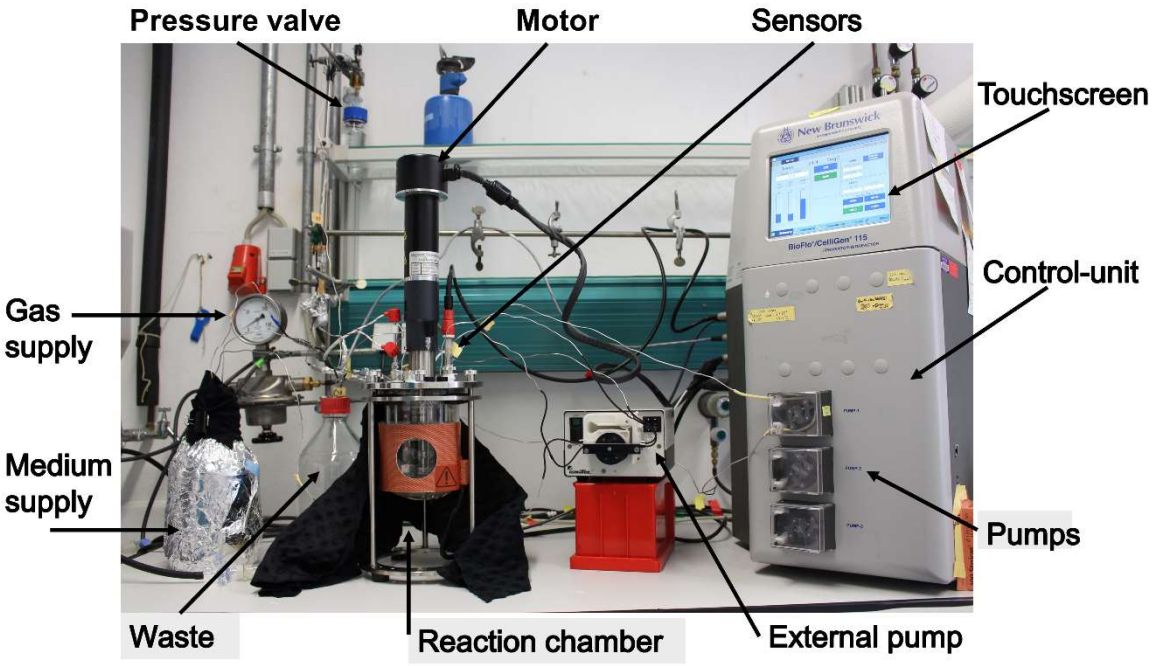


738

739 **Figure S2:** Logged data collected for temperature, pH and DO (dissolved oxygen) over time in
740 the chemostat reaction chamber.

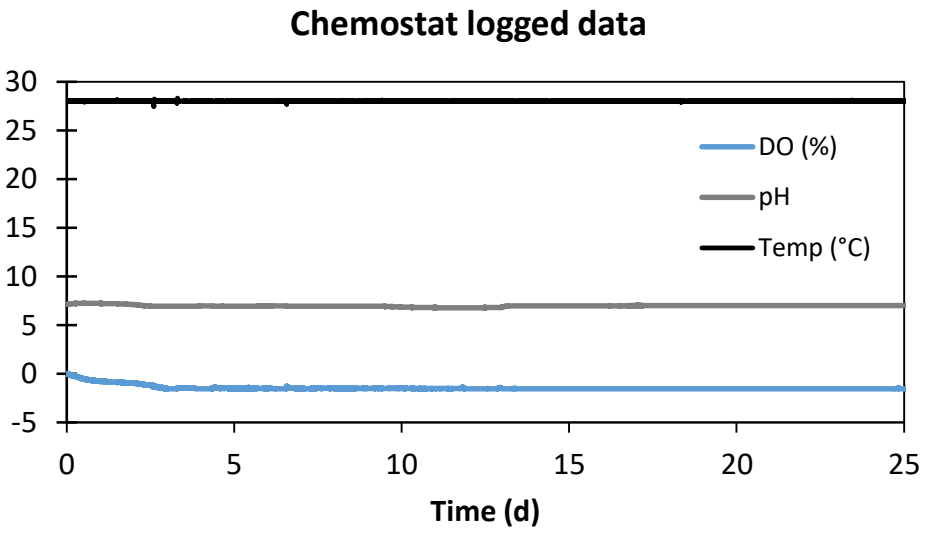


741

**Figure S3: Fe(II) oxidation in the chemostat.** Oxidation rates were calculated by first measuring the Fe(II) concentration $[Fe(II)_{meas}]_{t(0\ and\ 1)}$ in the reactor for the first two timepoints, where no pumping was turned on yet. Then, to account for mixing (dilution) effects , the expected Fe(II) concentration ($[Fe(II)]_{expected,t(x+1)}$; i.e. what we would be expected if there was no microbial Fe(II) oxidation and only addition and mixing of Fe(II) from the supplied medium (supplied: 2.82 mM $Fe(II)_{aq}$ and 7.38 mM $Fe(II)_s$) was calculated. The difference between $[Fe(II)_{meas}]_{t(x+1)}$ (with x ≥ 1) and $[Fe(II)]_{expected,\ t(x+1)}$ thus indicated how much Fe(II) was oxidized microbially over a given time period.

The rate of microbial oxidation of Fe(II) in the chemostat was therefore calculated according to equations 1 and 2.

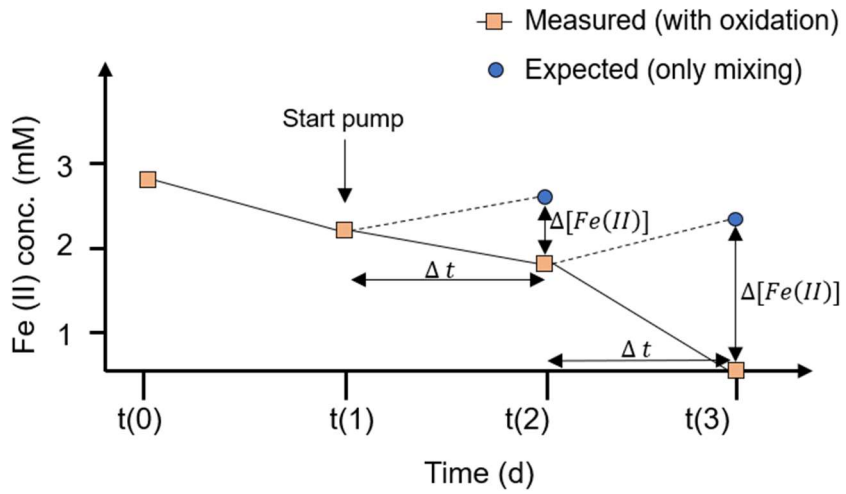


$$\frac{d[Fe(II)]}{dt} = \frac{[Fe(II)_{expected}]_{t(x+1)} - [Fe(II)_{meas}]_{t(x+1)}}{\Delta t} \quad \text{eq. 1}$$

Where $\Delta t$ is the difference in time between two measured points t(x+1) and t(x).

$$[Fe(II)_{expected}]_{t(x+1)} = [Fe(II)_{meas}]_{t(x)} \frac{(V_{chem} - (R_{addition} \Delta t))}{V_{chem}} + [Fe(II)_{sup}] \frac{R_{addition} \Delta t}{V_{chem}} \quad \text{eq. 2}$$

Where $V_{chem}$ is the volume of the chemostat (700 ml); $R_{addition}$ is the flow rate of medium supplied to the chemostat (15 ml $h^{-1}$); $[Fe(II)_{sup}]$ is the concentration of Fe(II) added into the chemostat by pumping (2.82 mM $Fe(II)_{aq}$ and 7.38 mM $Fe(II)_s$ respectively. Note that x ≥ 1 (since pumping did not start until after t(1)).

The equation for the expected concentration $[Fe(II)_{expected}]_{t(x+1)}$ accounts for the mixing of Fe(II) already present in the chemostat $[Fe(II)_{meas}]_{t(x)}$ by medium supplied to the

761 chemostat $[Fe(II)_{sup}]$ (constant). Medium was supplied at a pumping rate of 15 ml $h^{-1}$. Every
762 24 h, 360 ml of $[Fe(II)_{sup}]$ was added to 340 ml of $[Fe(II)_{meas}]_{t(x)}$, which remained from
763 the previous time point, reaching a total volume of 700 ml in the chemostat. The difference
764 between the measured concentration $[Fe(II)_{meas}]_{t(x+1)}$ and the expected concentration
765 $[Fe(II)_{expected}]_{t(x+1)}$ corresponds to the amount of Fe(II) oxidized between t(x) to t(x+1).
766 Calculations were performed separately for $Fe(II)_{aq}$ and $Fe(II)_{s}$.

767

768 **Figure S4: Batch experiments performed as control: small volume (25 ml), shaken at 50 rpm.**
769 Fe(II) (circles) and Fe(III) (squares) measured in aqueous (grey) and solid phase (orange) during
770 cultivation of culture KS with 10 mM Fe(II) and 4 mM of $NO_3^-$ in three bottles A, B, and C which
771 represent biological replicates. D: abiotic control.

772

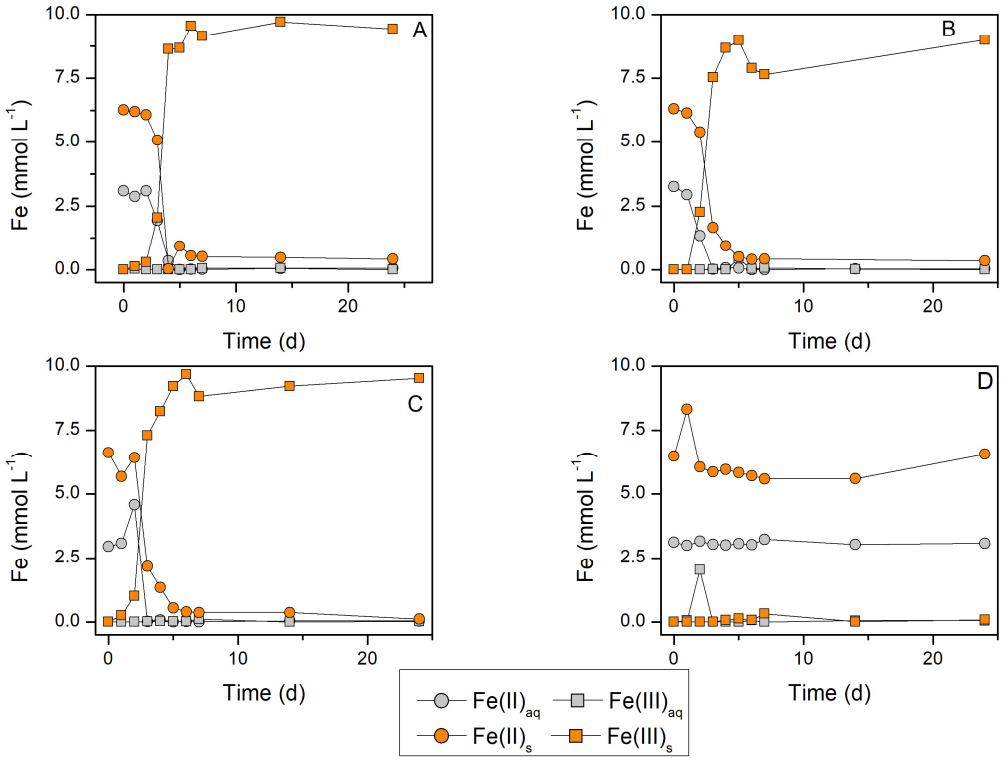

773 **Figure S5: Batch experiments performed as control: small volume (25 ml), static.**
774 Fe(II) (circles) and Fe(III) (squares) measured in aqueous (grey) and solid phase (orange) during
775 cultivation of culture KS with 10 mM Fe(II) and 4 mM of $NO_3^-$ in three bottles A, B, and C which
776 represent biological replicates. D: abiotic control.

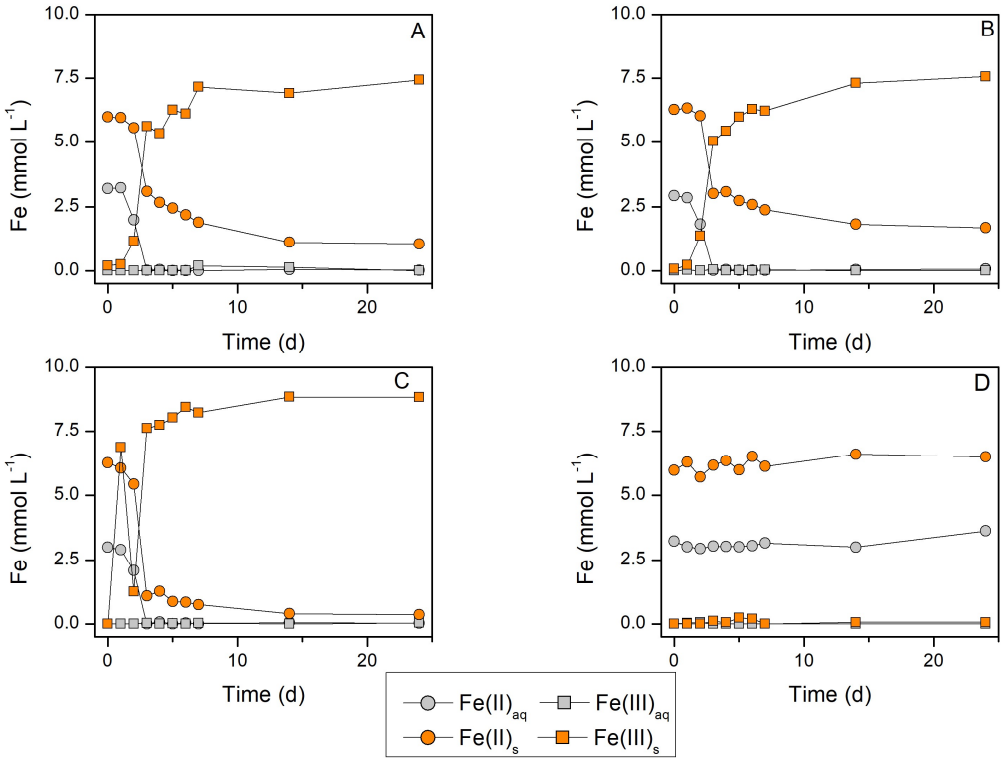


777

**Figure S6: Batch experiments performed as control: big volume (700 ml), shaken at 50 rpm.** Fe(II) (circles) and Fe(III) (squares) measured in aqueous (grey) and solid phase (orange) during cultivation of culture KS with 10 mM Fe(II) and 4 mM of $NO_3^-$ in three bottles A, B, and C which represent biological replicates. D: abiotic control.

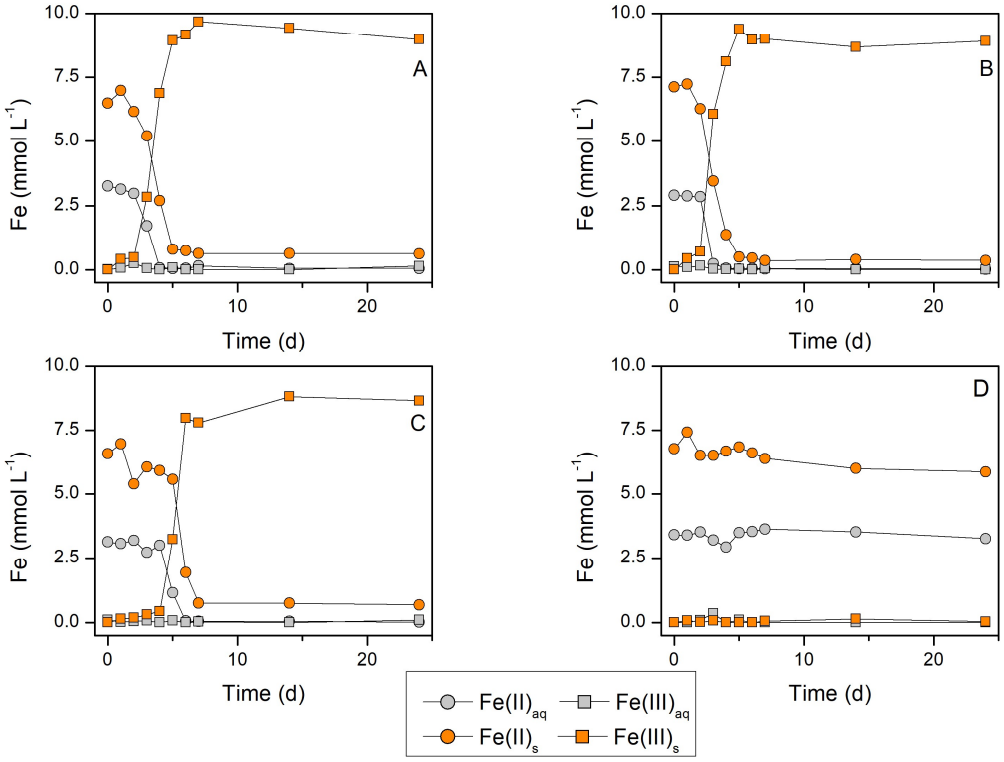

**Figure S7: Batch experiments performed as control: big volume (700 ml), static.** Fe(II) (circles) and Fe(III) (squares) measured in aqueous (grey) and solid phase (orange) during cultivation of culture KS with 10 mM Fe(II) and 4 mM of $NO_3^-$ in three bottles A, B, and C which represent biological replicates. D: abiotic control.

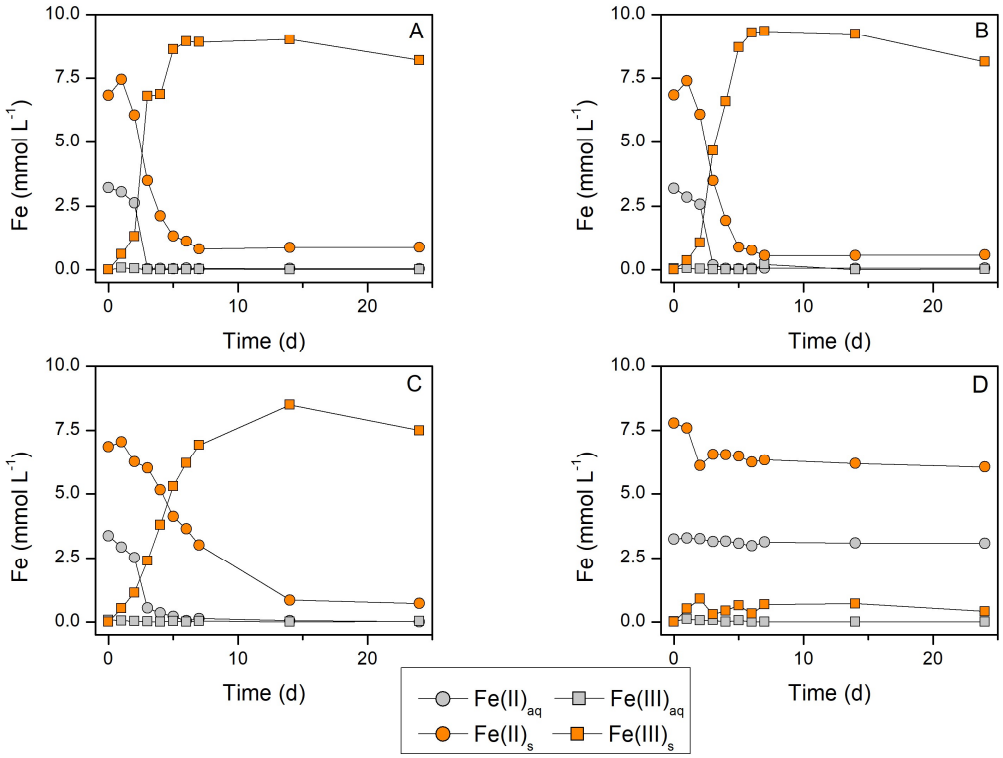

**Figure S8: Batch experiments performed as control: small volume (25 ml), shaken at 50 rpm.** $NO_3^-$ (black circles) and $NO_2^-$ (blue circles) measured in aqueous phase during cultivation of culture KS with 10 mM Fe(II) and 4 mM of $NO_3^-$ in three bottles A, B, and C which represent biological replicates. D: abiotic control. **Note differences in y-axes scale to better show the variance in the biological data.**

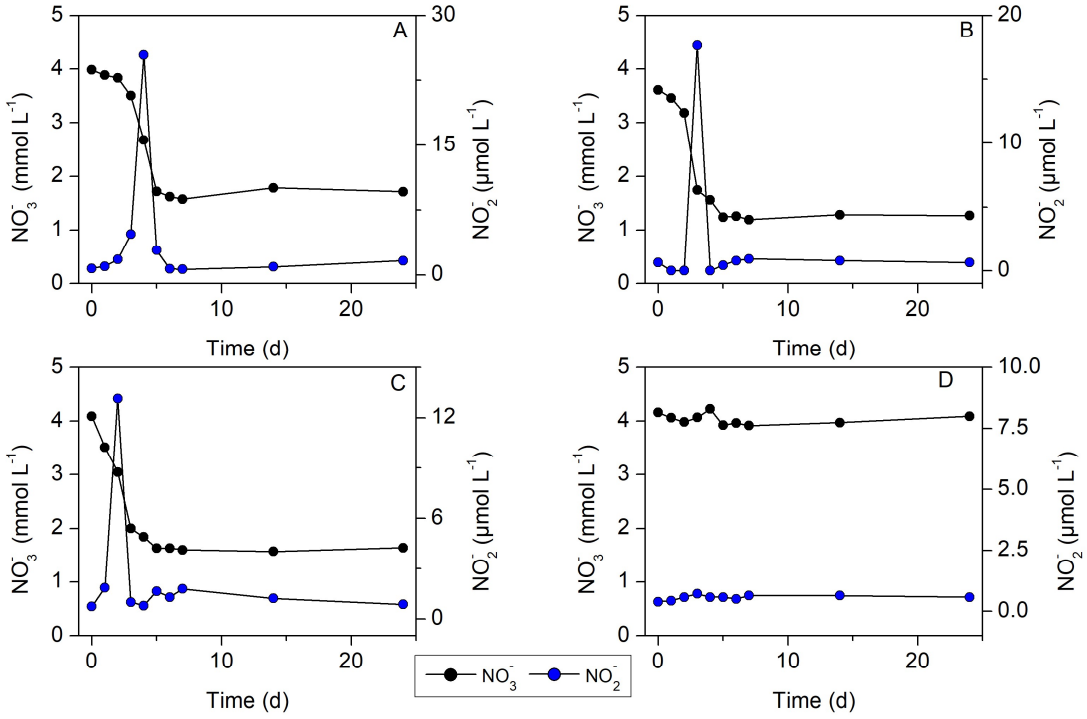

797 **Figure S9: Batch experiments performed as control: small volume (25 ml), static.**
798 $NO_3^-$ (black circles) and $NO_2^-$ (blue circles) measured in aqueous phase during cultivation of
799 culture KS with 10 mM Fe(II) and 4 mM of $NO_3^-$ in three bottles A, B, and C which represent
800 biological replicates. D: abiotic control. **Note differences in y-axes scale to better show the**
801 **variance in the biological data.**

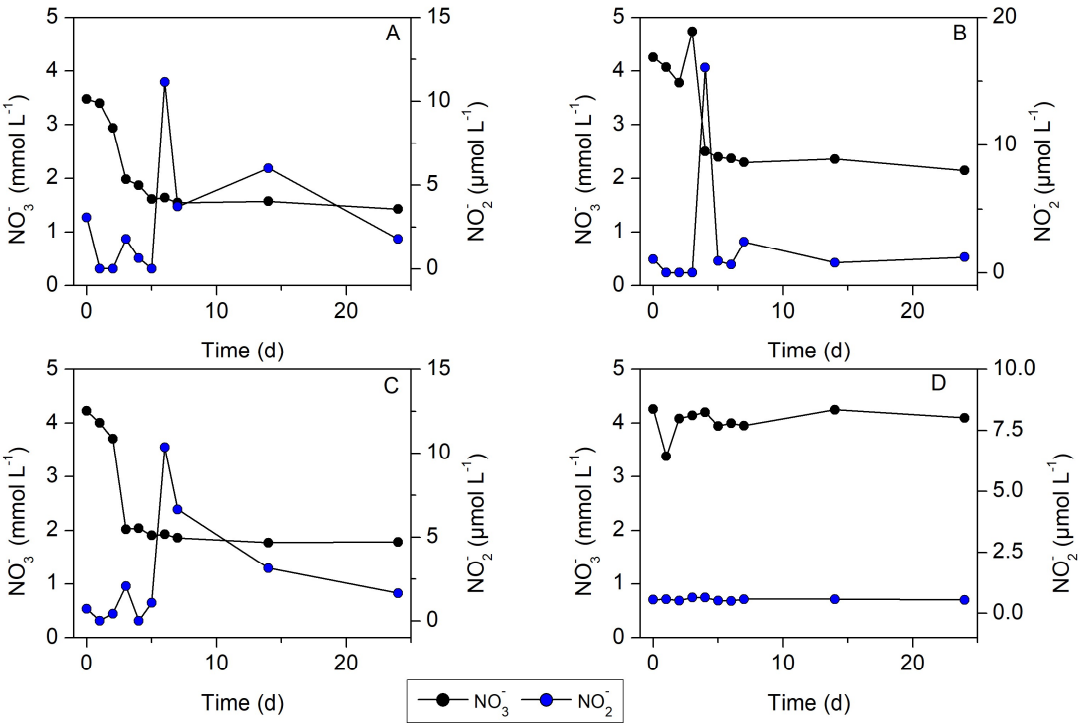


802

803

804 **Figure S10: Batch experiments performed as control: big volume (700 ml), shaken at 50 rpm.**
805 $NO_3^-$ (black circles) and $NO_2^-$ (blue circles) measured in aqueous phase during cultivation of
806 culture KS with 10 mM Fe(II) and 4 mM of $NO_3^-$ in three bottles A, B, and C which represent
807 biological replicates. D: abiotic control. **Note differences in y-axes scale to better show the**
808 **variance in the biological data.**

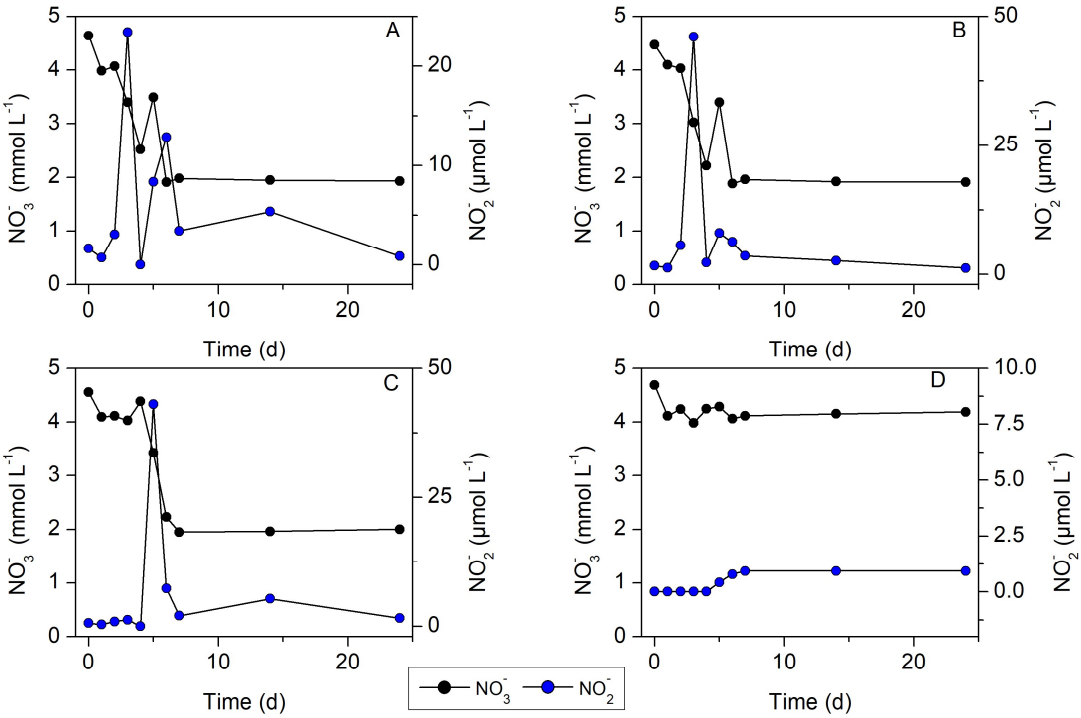


809

810

**Figure S11: Batch experiments performed as control: big volume (700 ml), static.** $NO_3^-$ (black circles) and $NO_2^-$ (blue circles) measured in aqueous phase during cultivation of culture KS with 10 mM Fe(II) and 4 mM of $NO_3^-$ in three bottles A, B, and C which represent biological replicates. D: abiotic control. **Note differences in y-axes scale to better show the variance in the biological data.**

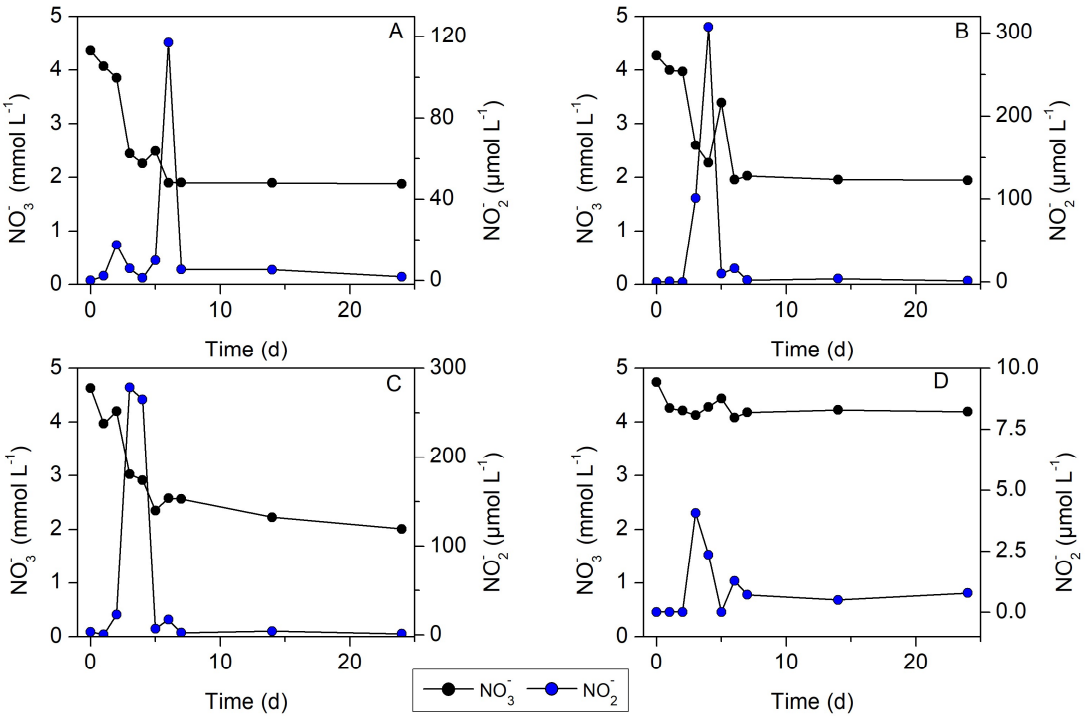

818 **Figure S12**. µ-XRD patterns for collected and oven dried minerals precipitates from (a) 25 ml
819 and (b) 700 ml batch experiments (both shaken), as well as chemostat samples collected at (c)
820 timepoint 7 (*chem1*) and (d) 24 days (*chem2*) of autotrophically growing culture KS with 10
821 mM Fe(II) and 4 mM of nitrate. Noise at 2-Theta of approx. 51° and 65° is due to the sample
822 holder (Si-wafer). Ha: halite, Ho: sample holder, W: wuestite, V: vivianite.

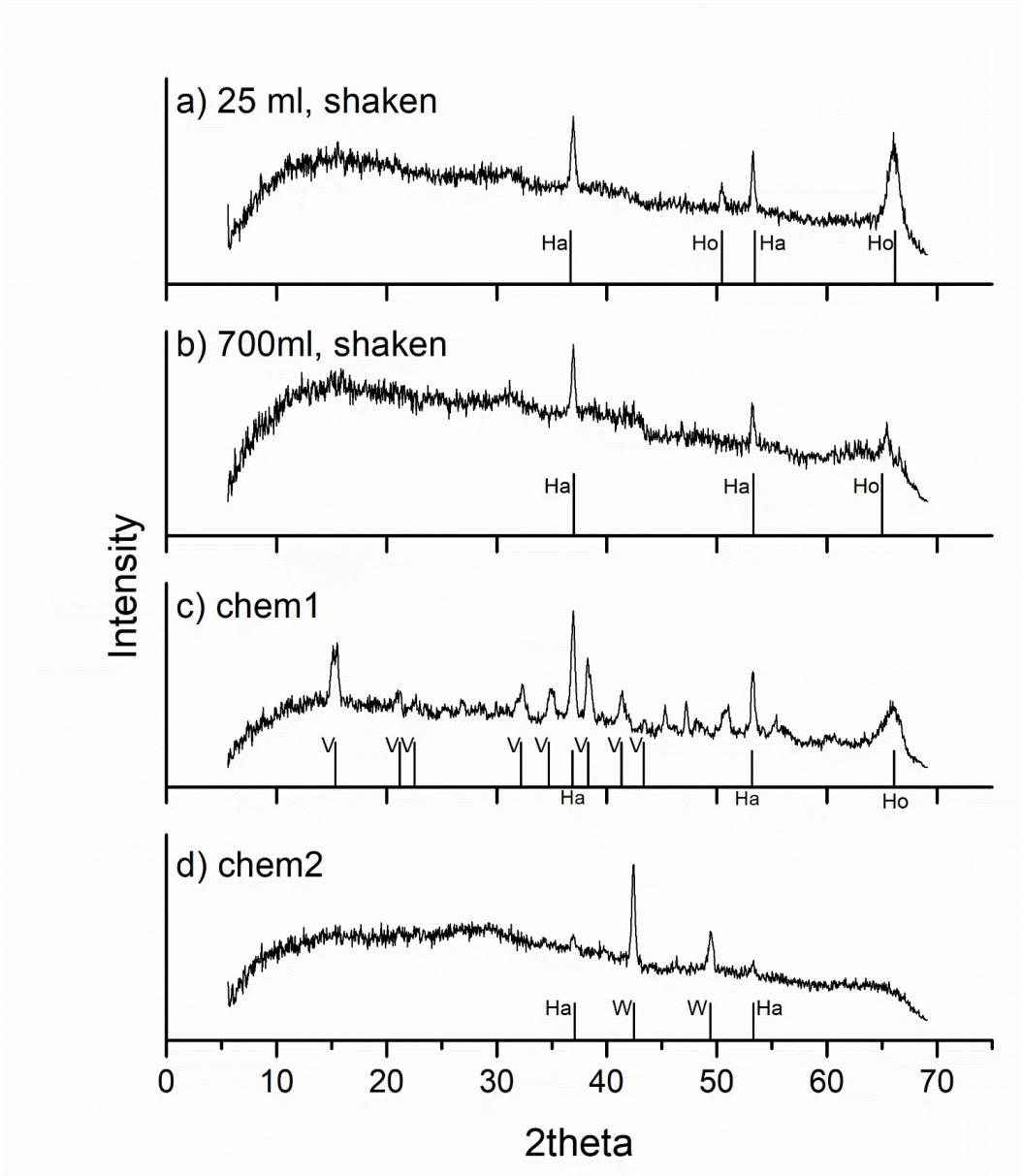

823 **Figure S13.** X-ray absorption spectroscopy analysis of collected mineral precipitate collected
824 from the very bottom of the chemostat bioreactor, after continuous cultivation of
825 autotrophically grown culture KS for 40 days with 10 mM Fe(II) and 4 mM of nitrate. Recorded
826 values and fitted data are displayed in solid and dashed lines respectively.

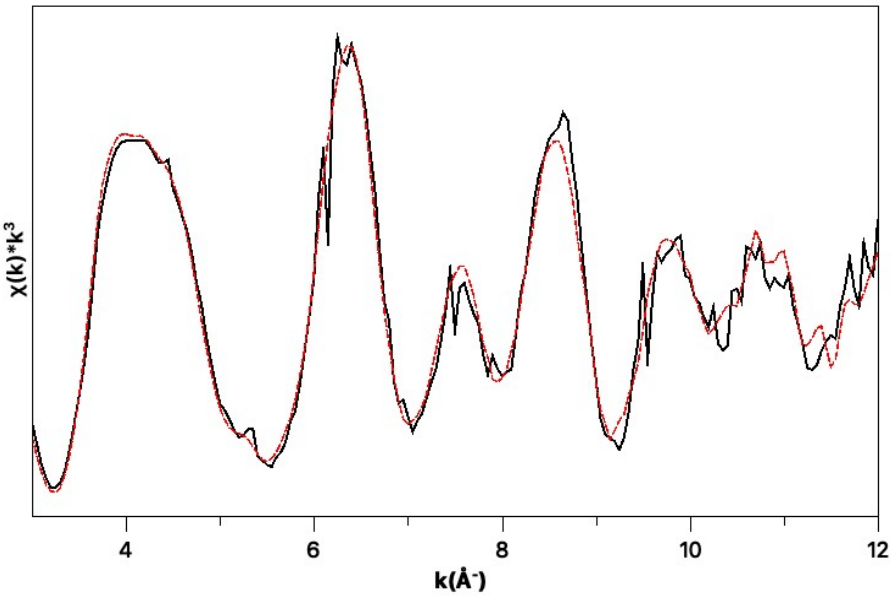


827

828

**Figure S14.** Composition of collected mineral precipitate sample from the very bottom of the chemostat bioreactor (analysed with X-ray absorption spectroscopy), after continuous cultivation of culture KS grown autotrophically for 40 days with 10 mM Fe(II) and 4 mM of nitrate.

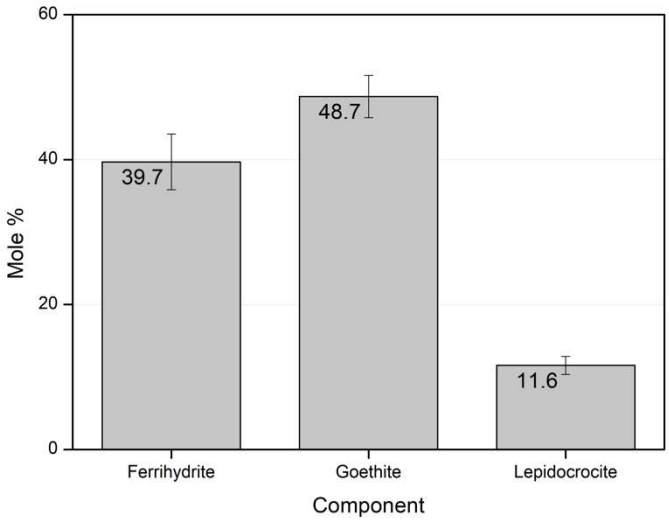

834 **Figure S15.** Relative amount of not, partially, or completely encrusted cells investigated and
835 counted with scanning electron microscopy from continuous cultivation of culture KS under
836 autotrophic conditions in the chemostat. A total of 78 cells were counted from the
837 chemostat.

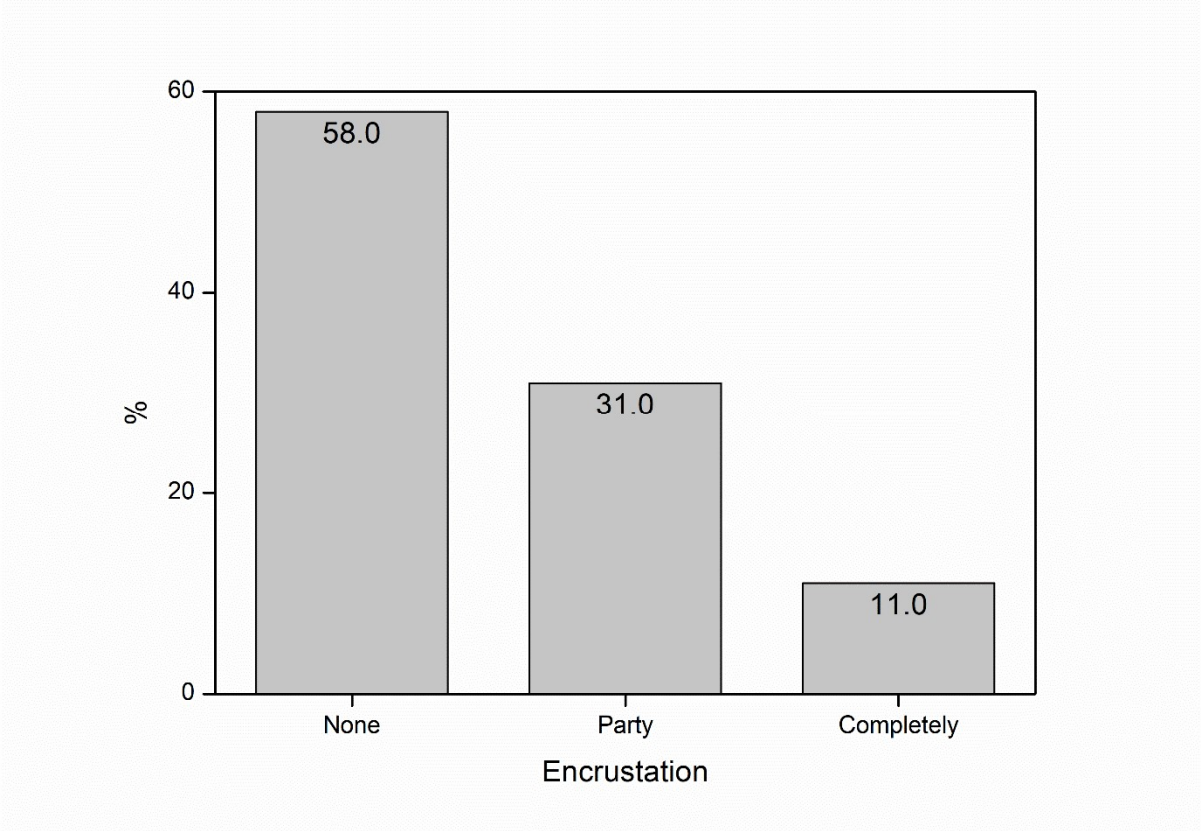


838
839
840

841 **Figure S16.** Fluorescence microscopy images of culture KS grown autotrophically with 10 mM
842 Fe(II) and 4 mM of nitrate in the chemostat at day 24. Green colours represent live cells while
843 magenta colours show dead cells. Cells were stained with D/L stain.
844

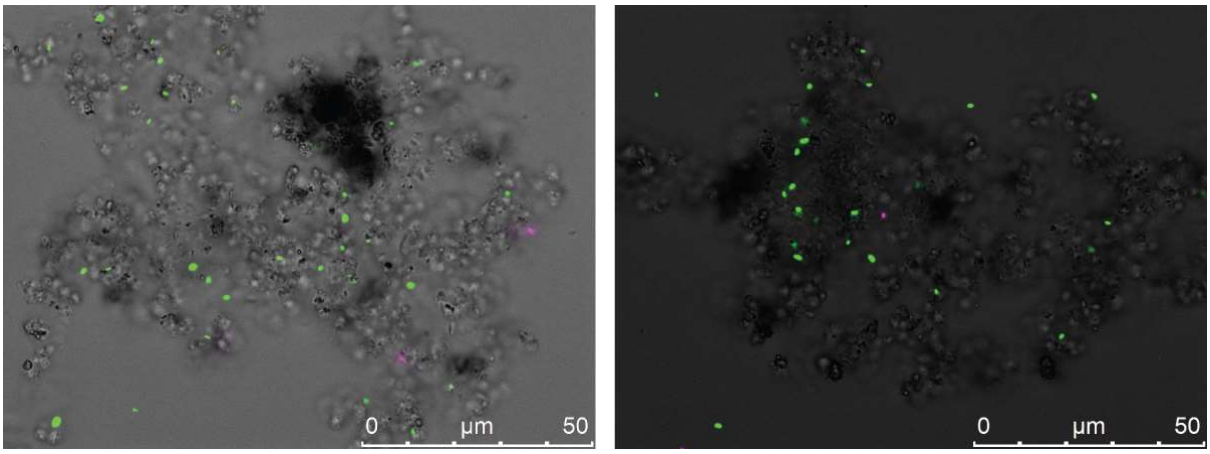


845
846
847

848 **Table S1.** Recorded values for Mössbauer spectroscopy measured at 77 K for samples collected
849 from the chemostat during continuous cultivation of autotrophically grown culture KS with 10
850 mM Fe(II) and 4 mM of nitrate. δ – isomer shift, $\Delta E_Q$ – quadrupole splitting, $\sigma(\Delta E_Q)$ – standard
851 deviation of $\Delta E_Q$, R.A. – relative spectral area, Reduced (Red.) $X^2$ – goodness of fit.

| Sampling timepoint (days) | Oxidation state | δ (mm/s) | $\Delta E_Q$ (mm/s) | $\sigma(\Delta E_Q)$ (mm/s) | R.A. (%) | error (%) | Red. $X^2$ |
|---|---|---|---|---|---|---|---|
| 0 | Fe(II) | 1.34 | 2.56 | 0.46 | 71.3 | 6.2 | 0.57 |
| | Fe(II) | 1.32 | 3.26 | 0.03 | 22.7 | 6.3 | |
| | Fe(III) | 0.38 | 0.79 | 0.17 | 6.0 | 1.9 | |
| 3 | Fe(II) | 1.25 | 3.00 | 0.18 | 9.2 | 1.3 | 0.75 |
| | Fe(III) | 0.49 | 0.79 | 0.30 | 90.8 | 1.3 | |
| 7 | Fe(II) | 1.23 | 3.09 | 0.25 | 7.3 | 2.1 | 0.69 |
| | Fe(III) | 0.49 | 0.80 | 0.31 | 92.7 | 2.1 | |
| 14 | Fe(II) | 1.26 | 2.95 | 0.28 | 18.3 | 4.0 | 0.63 |
| | Fe(III) | 0.50 | 0.75 | 0.29 | 81.7 | 4.0 | |
| 24 | Fe(II) | 1.15 | 2.84 | 0.13 | 5.1 | 2.9 | 0.60 |
| | Fe(III) | 0.49 | 0.82 | 0.33 | 94.9 | 2.9 | |

852

853

854 **Table S2:** Results of unpaired t-test for differences treatments.

| Phase | Comparison | t | df | p-value |
|---|---|---|---|---|
| *NA* | Aqueous vs solid | -3.4161 | 13.589 | 0.00434 |
| Aqueous | Big vs small | 1.2745 | 8.6747 | 0.2356 |
| Aqueous | Static vs shaking | -1.0946 | 8.8422 | 0.3026 |
| Solid | Big vs small | -2.5091 | 9.9184 | 0.03114 |
| Solid | Static vs shaking | 1.7128 | 9.8305 | 0.1181 |

855

856

857

858